T H E U N I V E R S I T Y O F T U L S A

THE GRADUATE SCHOOL

THE EFFECT OF CARBON NANOTUBES ON THE RHEOLOGY AND MECHANICAL PROPERIES OF LIGHTWEIGHT CEMENTS

by
Xin Li

A thesis submitted in partial fulfillment of

the requirements for the degree of Master of Science]

in the Discipline of Petroleum Engineering

The Graduate School

The University of Tulsa

2017

THE UNIVERSITY OF TULSA

THE GRADUATE SCHOOL

THE EFFECT OF CARBON NANOTUBES ON THE RHEOLOGY AND MECHANICAL PROPERIES OF LIGHTWEIGHT CEMENTS

by
Xin Li

A THESIS

APPROVED FOR THE DISCIPLINE OF

PETROLEUM ENGINEERING

By Thesis Committee

Stefan Miska, Chair
Nicholas Takach, Co-Chair
Evren Ozbayoglu
Mengjiao Yu

COPYRIGHT STATEMENT

ABSTRACT

Xin Li (Master of Science in Petroleum Engineering)

The Effect of Carbon Nanotubes on the Rheology and Mechanical Properties of Lightweight Cements

Directed by Dr. Stefan Miska

103 pp., Chapter 6: Conclusions and Recommendations

(285 words)

Oil wells drilled in weak and fragile formations should be cemented by lightweight cement slurries to avoid downhole fractures caused by heavy slurry and to minimize lost circulation. Conventional cement composite is a strong material with low elasticity due to its brittle nature. Lightweight cement sheath exhibits higher ductility than conventional cement because its air-solid structure is able to tolerate more deformation when downhole stress condition changes. The addition of foam and microspheres into conventional cement introduces higher elasticity, it also reduces the strength properties.

In this study, multi-walled carbon nanotubes were employed to compensate for strength reduction caused by foam and microspheres in cement composites. The goal of this study is to evaluate the mechanical properties of CNT reinforced lightweight cements under tri-axial conditions. Rheological properties of various cement systems were measured.

Compressive strength and Young's modulus of lightweight cements were measured under the confining pressures of 0, 500 psi and 1000 psi. Permeability and porosity tests were conducted on various cement systems. The strength properties of cement specimens were evaluated by their

compressive strength and splitting tensile strength. Several failure criteria were applied to describe cement failure mechanism. Young's modulus, ultimate strain capacity and brittleness index were measured and calculated for the analysis of cement elastic properties. A scanning electron microscope was used for the comparison of micro structures among cement systems and prove the bridging mechanism of carbon nanotubes in cement composite.

As shown in experimental results, the addition of carbon nanotubes improves the strength and elastic properties of various cement systems without significantly affecting their rheological properties. Carbon nanotubes function as nano-bridges and nano-fillers to help reinforce cement composite and plug the mico pores and cracks for hydrocarbon to flow through.

ACKNOWLEDGEMENTS

I would like to thank my advisor, Dr. Stefan Miska, for giving me the opportunity to work on this cement project and providing support during my study in the University of Tulsa Drilling Research Projects Group (TUDRP). I would like to thank Dr. Nicholas Takach, Dr. Mengjiao Yu, and Dr. Evren Ozbayoglu for their invaluable guidance, suggestion, and encouragement throughout my graduate study. I would also like to thank Mrs. Paula Udwin for her kindly help. Appreciation is extended to Mr. Randy Darden and Mr. Timothy Smith for their technical support in laboratory.

I would like to acknowledge Mr. Mark Meade from Schlumberger for the donation of cement chemicals, Dr. Clara Mata from 3M for providing microspheres and sharing expertise, and Mr. Rick Portman from the Biology Department at The University of Tulsa for helping me with scanning electron microscope tests. Special thanks also go to Dr. Saeed Rafieepour for the training on the Tri-axial facility, and other TUDRP colleagues for their friendship and help.

I sincerely thank my parents for their understanding and encouragement. I would like to dedicate this thesis to my wife, Jiajing Li, for her love and support.

TABLE OF CONTENTS

LIST OF FIGURES

INTRODUCTION

Cementing a well is an important process in oil well drilling, which requires to maintain wellbore mechanical integrity and effective zonal isolation through the life of an oil well. A poor cementing job may result in cement sheath crack and failure, oil and gas migration behind the casing, shorten the well life and even well abandonment. A successful cementing job needs to place cement slurry effectively in the annulus to get better cement to casing and formation bonds, which restricts hydrocarbon channeling and provides mechanical support for the casings. Lost circulation control of cement slurry is another important issue in a cementing job.

The high density of conventional cement slurry results in high downhole hydrostatic pressures, which put the downhole section of a wellbore at high risk of being fractured by heavy cement slurry. Especially, for drilling in fragile and highly permeable formations, low density cement slurries are required to avoid downhole fractures and minimize lost circulation. Several methods are being used in industry to reduce cement density, such as aerating slurry, adding microspheres or simply adding extra water and water extenders. However, lowering the density of conventional cement slurry by adding water or water extenders results in significant decrease in compressive strength and increases the wait-on-cement time [1].

Lightweight cement, unlike conventional cement, is a mixture of base cement slurry, low density additives (air, micro glass spheres, etc.) and chemicals (surfactant, retarder, etc.). The low density makes lightweight cement highly applicable in low-fracturing-pressure gradient zones, such as fragile formations, depleted reservoirs, highly permeable reservoirs and deep water well drillings [2].

The application of foam cement in petroleum industry dates back to 1980s [3]. Foam cement consists of conventional cement slurry, gas, and foaming chemicals (foaming agent and foam stabilizer). As discussed by Ahmed et al, 2009 [4], foam cement slurry is more viscous than its base (non-foamed) slurry. Compared to conventional (non-foamed) cement, foam cement slurries have better mud removal ability, lost circulation control, and cement displaceability, which improves zonal isolation and decreases fluid loss in highly permeable formations. The entrained gas bubbles enable a foam cement sheath to store more deformation than solid cement material, resulting in a lower Young's modulus, higher strain capacity, and increased resistance to underground stresses [5][6]. However, hardened foam cement has lower compressive strength than conventional cement, due to its air-solid structure. Because gas bubbles are dispersed in the continuous cement slurry, foam cement slurry is compressible and unstable, which makes its foam quality and rheology varied with fluid circulation and well depth. As foam cement slurry goes deeper into the wellbore, increased temperature and pressure change the foam quality and rheology.

Another lightweight technique is using microspheres as cement extenders. Microspheres, commonly known as hollow glass spheres, are incompressible density reduction agents with high crush strength (2000-18000 psi), small particle size (1-100 μm), and low density (0.29-0.63 g/cc). Compared to foam cement slurry, microsphere cement slurry is stable and incompressible. The viscosity and yield stress of microsphere cement slurry varies with the concentration and surface areas of microspheres [7]. Dry blend (pre-blend) of cement powder, microspheres, together with other solid chemical additives, is commonly used to maximize the packing density of solids and minimize the amount of water to prepare the slurry [8]. The strength of set microsphere cement is affected by the type of microspheres and increases with cement volume fraction [9]. A number of

laboratory tests indicate that properly designed microsphere cement slurries acquire high strength to density ratio and low permeability [10].

Carbon nanotubes, known as the strongest and stiffest nano-fibers in terms of strength and elasticity, have been widely used in industry to improve material strength properties. Multi-walled carbon nanotubes have been reported to have tensile strength and ultimate tensile strain as high as 40 GPa and 12%, respectively [11], which is ideal for use to reinforce the strength properties of lightweight cement composite.

CHAPTER 1

PROBLEM STATEMENT AND OBJECTIVES

1.1 Problem Statement

Cement is a brittle material with low elasticity, which is unable to withstand big downhole stress changes and deformations, resulting from dynamic loading of wellbore, seismic activities, casing thermal expansion, etc. The sources of dynamic loading of wellbore include surge and swab pressures during tripping operation, drillstring vibration, hydraulic fracturing, and unsteady flow during production, etc. Seismic activities constantly happen in the oil fields caused by reactivation of pre-existing faults resulting from reservoir depletion and enhanced oil recovery. Furthermore, as temperature increases with well depth, casing, cement sheath, and formation deform to different degrees at different rates due to different thermal expansion coefficients during cement injection and wait-on-cement period. After cement slurry is fully set in annuli, the thermal expansions will inevitably result in initial stress conditions in cement sheath.

Design of a new cement system, which can exhibit more strain capacity and tolerate more deformations, is important to ensure wellbore integrity and elongate well life. Lightweight cement, due to its air-solid structure, shows higher strain capacity than its solid phase. However, its strength properties are relatively lower than those of conventional cement. In this study, carbon nanotubes are mixed into lightweight cements to compensate strength loss caused by aerating or adding microspheres.

Extensive research have shown that carbon nanotubes improve cement paste properties include (1) early-stage and long-term compressive strength improvement [12][13][14][15], (2)

viscosity increase [16], and (3) cement slurry hydration acceleration [17]. However, studies on the integrity of CNT-reinforced cements under actual downhole conditions are limited. In this study, the compressive strength and Young's modulus of CNT-reinforced lightweight cements were evaluated under tri-axial conditions. Permeability and splitting tensile strength of lightweight cements were measured and compared to their base phases. Scanning Electron Microscopy (SEM) was employed to analyze the dispersion of foam, microspheres and CNTs in cement composites.

Moreover, the rheology of CNTs reinforced lightweight cement slurries were measured and compared with empirical models.

1.2 Objectives

The main objectives of this project are

- Perform experiments to validate the effect of CNTs on lightweight cement strength enhancement.
- Conduct tri-axial experiments to study the effect of CNTs on improving cement mechanical properties (i.e. compressive strength, Young's modulus, Poisson's ratio, strain capacity, brittleness, and permeability) under conditions that simulate actual downhole pressures.
- Design experiments to measure the splitting tensile strength of cement specimens.
- Compare the permeability and porosity of foam and microsphere cement systems.
- SEM analysis of the micro structures of different lightweight cement systems, i.e. foam cement, microsphere cement and water extended cement, and CNTs' bridging and plugging in cement composite.

- Modify current rheology testing system and design experiments to study the effect of CNTs on cement rheology under flow-through conditions. Apply empirical model to characterize the rheology of cement slurries.

CHAPTER 2

LITERATURE REVIEW

2.1 Foam Cement

R.M. Ahmed et al. (2008) [4] measured the rheology of foamed cement by changing the foam quality under different pressure conditions. This study shows that viscosity of foam cement slurry increases as the foam quality increases from 10% to 30%. The viscosity of foam cement slurry is higher than its base non-foamed phase, but low-quality cement foams exhibit less viscosity than its base phase.

Olowolagba and Brenneis (2010) [18] designed a new equipment, referred to as the Fann Yield Stress Adapter (FYSA), for the study of foamed cement rheology, which is able to maintain a homogenous mixture and minimize wall slip during rheology measurement. The result shows that the viscosity and yield points of foamed cements are higher than non-foamed base slurries, and are increases with foam quality.

Griffith et al. (2004) [19] discussed the optimum foamed cement sheath properties for maintain wellbore integrity under high pressure high temperature (HPHT) conditions, by analyzing some case examples of foam cement and conventional cement wells in Norwegian and North Sea. The comparison of foamed and non-foamed cement wells shows that foamed cement has better displacement efficiency and long-term zonal isolation under HPHT conditions.

Dusterhoft (2003) [20] compared foam cement with ceramic spheres lightweight cement with the densities of 1200kg/m3, 1300kg/m3 and 1400kg/m3. Results show that foam cement and lightweight cement have similar strength properties. The density and permeability of foam cement

varies throughout the well, while the density and permeability of ceramic sphere lightweight cement remains constant at different sections in an oil well.

Kopp et al. (2000) [5] analyzed the data from six deep wells cemented by 8.8 lb/gal foam cement in Wyoming. The data of case examples indicates that foam cement has better displacement quality and is capable to cement deep liners more effectively than conventional cement. Foam cement costs approximately 30% more than that of conventional cement, lightweight cement on a cost per cubic foot basis.

Spaulding et al. (2015) [21] measured the Young's modulus, Poisson's ratio and permeability of atmospherically generated foam cements under cyclic confining pressures. Results indicate that cyclic pressure significantly decreases the permeability, while showing negligible effect on Poisson's ratio. Young's modulus decreases with increased foam quality. Mechanical properties of foam cement are greatly affected by the first pressure cycle.

Kutchko et al. (2014) [22] conducted experiment on foam cement produced in atmospheric laboratory and high-pressure field conditions. Results of the laboratory produced foam cement indicates that porosity and permeability are increasing with foam quality, compressive strength and Young's modulus are decreasing with foam quality. The comparison of atmospheric and field high pressure generated foam cements indicate that atmospheric generated foam cement has larger, more uniform and evenly distributed bubbles, while field high-pressure generated foam cement has smaller and variable bubble sizes.

2.2 Microsphere Cement

Microspheres are small spherical particles with diameters in micro scale. Microspheres can be classified as glass microspheres, polymer microspheres, ceramic microsphere, mental microspheres, etc. Hollow glass microspheres (HGS), consist of ultra-strong glass wall and inner hollow space, have been used in petroleum industry to reduce the density of drilling fluids and cementing fluids. A cement slurry light-weighted by HGS shows lower compressibility than water-extended and foamed slurry, resulting in a stable cement system that has better downhole hydrostatic pressure control.

2.2.1 Microsphere Cement Applications in Petroleum Industry

Mata and Calubayan (2016) [9] prepared lightweight cement slurries using different kinds of hollow glass spheres with the same water ratio of 50% vol. The compressive strength results indicate that compressive strength of hardened cement samples increases with cement volume fraction. Cement slurries light-weighted by different kinds of hollow glass spheres have different strength properties.

Sarmah et al. (2015) [23] tested and compared two different kinds of lightweight cement systems, i.e. glass microspheres cement and ceramic microspheres cement. Test results indicate that glass beads outperform ceramic spheres on slurry stability, resulting from their more predictable density behavior under downhole elevated pressures. High compressive strength can be obtained by optimizing the concentration of cement powder, water and microspheres.

Veisi et al. (2015) [24] studied the lost circulation problem in the wells cemented by lightweight cement slurries. The lost circulation and sustained casing pressure were reduced, and cement bonding quality was improved by the addition of microspheres into cement slurries.

Blake et al. (2015) [25] compared two case examples in Mission Canyon, which is well known for its naturally fractured downhole condition and unpredictable weak formations. The two wells were cemented by hollow sphere lightweight cement and fiber based LCM (lost circulation material) cement, respectively. Well logging results indicate that both case wells achieved cement requirements successfully.

Tan et al. (2012) [26] investigated the oil wells, whose production casings were cemented by microsphere cement in Australia. Result shows that lower density microsphere cement maintains a high cement solid content, low permeability, and high compressive strength.

Kulakofsky et al. (2006) [27] presented several case studies in Mexico Cantarell offshore oilfield. Five offshore production wells cemented by foamed ultra-lightweight microsphere slurries with the density of 5.4 lb/gal achieved circulation and effective seal.

2.2.2 Hollow Glass Spheres Mechanical Properties

The stability of microspheres during slurry preparation and cement circulation under HPHT conditions determines the quality of a lightweight cement slurry. Generally, HGS bears high crush resistance. However, the mechanical properties are difficult to measure, due to their micro sizes.

Koopman et al. (2003) [28] designed a nano-compression test to measure the maximum load that a hollow glass bead (MB) is able to withstand. An example of a load-displacement curve from nano-compression test is given in Figure 2.1. The load-displacement curve is linear until the failure point (ultimate strength) of micro beads is reached. This is followed by a flat region, where micro glass beads keep cracking with negligible load increase, until one indenter imping reach the other. A single hollow glass sphere has been reported to have an ultimate strength in the range of 5 - 30mN, and Young's modulus in the range of 20 – 60 Gpa [29].

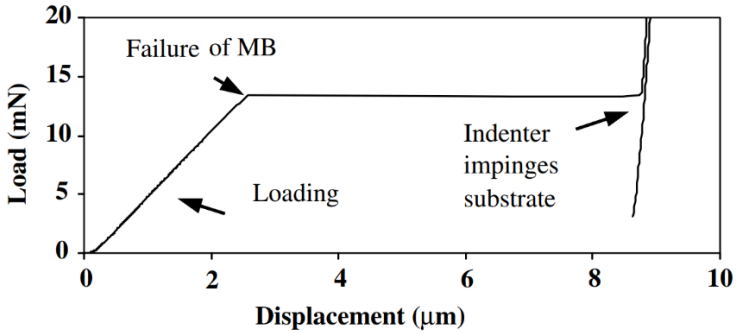

Figure 2.1 Compression behavior of hollow glass spheres [28]

In this study, microspheres used for preparing lightweight cement slurry were 3M HGS 8000x with ultimate crush resistance as high as 8000x, whose detailed physical properties are listed in Chapter 3.1.3.

2.3 Nano-engineered Cement Composite

2.3.1 Effect of Nano-materials on Foam Stability and Rheology

Hunter et al. (2008) [30] analyzed the effect of nanoparticles on acting as stabilizers or destabilizers. He proposed two stabilization mechanisms, i.e. particle detachment energy and maximum capillary pressure of coalescence. Particle detachment energy is significantly influenced by bubble surface areas, immersion angle, and surface tension. The detachment energy becomes higher, as surface tension (oil water surface) is lost due to particle absorption. The high detachment energy indicates more stable foams. Capillary pressure is the pressing force that brings two bubbles to one (coalescence). A higher capillary pressure indicates a more stable foam system.

Yang et al. (2006) [31] measured the viscosities of dispersions with different carbon-nanotubes (CNTs) concentrations. Result shows that viscosity varies with CNT concentrations at

low shear stress ($\tau < 1Pa$), while the viscosities of mixtures with different CNTs concentrations are similar at high shear stress ($\tau > 1Pa$).

Potschke et al. (2002) [32] analyzed the rheological behavior of multi-walled carbon nanotube (MWCNT) cement composite at the temperature condition of 260 ^{o}C. Results indicate that composite viscosity increases with MWCNT concentrations in the range of 0-15wt.% , and viscosity increment is accompanied with an increase in elastic properties.

2.3.2 Use of Nano-materials to Reinforce Cement Composite

Nazari and Riahi (2011) [33] improved the compressive strength of concrete specimens by over 70% with the addition of 4 wt.% SiO_2 nanoparticle. SiO_2 nanoparticles were used as nano-fillers in the pore spaces in concrete specimens.

Li et al. (2005) [34] investigated the effect of carbon nanotubes on cement mechanical properties in microstructure scale. Fourier Transform-Infrared Spectroscopy shows the chemical bonding between multi-walled carbon nanotube and cement matrix, which enhances cement flexural and compressive strength, as well as failure strain.

Khan et al. (2016) [15] used multi-walled carbon nanotubes (MWCNT) for enhancing mechanical properties of oil well cement under high pressure and high temperature conditions. This study shows oil well cement compressive strength improves as the concentration of multi-walled carbon nanotubes increases. Cement composite with 0.5 wt.% MWCNT exhibits the highest (15%) increase in compressive strength value.

Santra et al. (2012) [17] compared the effects of different kinds of nanomaterials on improving cement early strength development as accelerators. This study proved the ineffectiveness of CNT on enhancing the cement mechanical properties at atmosphere conditions.

Patil and Deshpande (2012) [35] analyzed the effect of temperature on the compressive strength of cement composite mixed with nanoparticles. They found that the ultimate compressive strength of cement composite mixed with nanoparticles can be greatly enhanced by increasing temperature.

Taiwo and Ogbonna (2011) [36] analyzed the application of foam cement in low-pressure gradient deep water operations. They pointed out that low density foam cement slurries are good to use in a low fracture gradient environment to reduce hydrostatic pressure on weak zones, leading to better zonal isolations.

Kawashima et al. (2013) [37] analyzed the effect of nanoparticles on cement-based materials. In this study, shear rheology results indicated that nanoclays have an immediate stiffening effect, governed by flocculation. Nano-$CaCO_3$ can be used to accelerate the rate of hydration and improve compressive strength.

CHAPTER 3

MATERIALS AND CEMENT PREPARATIONS

3.1 Materials

3.1.1 Cement Class H

According to API Specification 10A [38], oil well cements are classified into the following classes (A, B, C, D, E, F, G, and H) and grades (O, MSR and HSR), based on different application requirements. Class A cement is intended for general use without any required special properties. Class B cement has moderate to high sulfate corrosion resistance, which is highly suitable for cementing oil wells in sulfate rich reservoirs. Class C cement is capable to develop high early strength, while its long-term strength properties is in the same level as other cement classes. Class D cement is designed for use under moderate to high temperature and pressure conditions, while class E cement is good for use under high temperature and pressure conditions. Class F cement is designed for cementing extremely high temperature and pressure oil wells. Class H and G cements are basic and most common oil well cements without any additives other than calcium sulfate or water.

Cement used in this study is the most commonly used class H cement, which contents Portland cement, hydraulic calcium silicates, and calcium sulfate.

3.1.2 Carbon Nanotubes

Carbon nanotubes can be classified as single-walled carbon nanotubes (SWCNTs) and multi-walled carbon nanotubes (MWCNTs) in terms of their different layered structures. Single-walled carbon nanotubes consist of a one-atom-thick layer of graphene, while multi-walled nanotubes are composed of multiple concentric layers of graphene. The outer diameter of multi-walled carbon nanotubes varies from 5 nm to 80 nm, while its length is in the range of 10 μm to 50 μm, which is thousands or millions times over its outer diameter.

The physical properties of the multi-walled carbon nanotubes used in this study are summarized in Table 3.1.

Table 3.1 Physical properties of MWCNTs

Outer Diameter (nm)	Inner Diameter (nm)	Ash (wt%)	Purity (wt%)	Length (um)	Specific Surface Area (m2/g)	Bulk density (g/cc)	True Density (g/cc)
50-80	5-10	<1.5	>95	10-20	60	0.18	2.1

3.1.3 Hollow Glass Spheres (Type 8000x)

Hollow glass spheres, whose diameter varies from 10 to 300 micrometers, have high crush resistance ranging from 2000 to 18000psi. The high resistance allows greater survivability under HPHT downhole conditions. The microspheres used in this study are hollow glass spheres (HGS) type 8000x from 3M and their physical properties are shown in Table 3.2.

Table 3.2 Properties of HGS 8000x

Brand	Color	Composition	Crush Strength (psi)	Density (g/cc)	Particle size Range (um)
3M	White, Powdery	Soda-lime-borosilicate glass	8000	0.42	20-29

3.1.4 Cement Additives

Different cement chemical additives were mixed into cement base slurry to adjust slurry viscosity, setting time, dispersion, fluid loss, foam quality, etc. Fluid-loss additive, dispersant, retarder and foaming agent were used in the cement systems in this study.

The function of each cement chemical additive is summarized as follows:

- Retarder: Extend the cement slurry setting time and decelerate the hardening process.
- Dispersant: Reduce cement slurry viscosity, frictional pressure loss and improve flow behavior while flowing in drillpipe and annulus.
- Fluid-loss additive: Minimize the loss of aqueous phase in a cement system into formation, maintain a constant slurry density and pumpable state during cementing operation.
- Foaming agent: Generate and stabilize air bubbles in a foamed cement slurry.

  The concentration of each chemical additive is given in Table 3.

3.2 Cement Preparations

3.2.1 Preparation of Conventional and Lightweight Cement Slurries

Conventional, microsphere, and water extended cement slurries were prepared at ambient conditions in accordance with API RP10B-2 standard [39]. Foam cement slurries were prepared at ambient conditions in accordance with API RP 10B-4 standard [40]. A speed-programmable blender with bottom drive blades was used for slurry mixing process. Carbon nanotubes and microspheres were wetted and mixed with water in blender cup for better particle dispersion before adding into base slurry. A low mixing speed was used to minimize carbon nanotubes breakage and hollow glass sphere collapse. Cement powder and chemical additives were weighted and

thoroughly dry-blended before mixing. As recommended by API Spec 10A, class H cement slurry should be prepared with water at the amount of 38% by weight of cement (%bwoc). However, the viscosity of microsphere cement slurry would be too high to be pumpable in field application, if the water ratio keeps at 38%bwoc. To improve the pumpability of microsphere cement slurry, an elevated water ratio of 45% bwoc was used.

According to API RP 10B-2, a two-stage mixing procedure is recommended for slurry preparation. The pre-mixing stage requires to add cement powder and additives into water slowly and continuously in less than 15 second, while maintaining a constant rotational speed at 4000rpm. After all materials have been added into the mix water, seal the blender with cap and continue mixing at 12000rpm for 35 second. It should be noted that 12000rpm was applicable for both conventional and foam cement slurries. For microsphere cement slurry, a lower rotational speed of 4000rpm and a longer mixing time of 120s were used at stage two to minimize hollow glass sphere breakage and improve dispersion.

The density of lightweight cement slurry was measured by a fluid density balance (Figure 3.1) immediately after slurry preparation is done. The difference between measured density and target density of a cement slurry should be less than 2% of the total target density. Otherwise, the cement slurry should be discarded and a new patch needs to be prepared.

Figure 3.1 Density balance

3.2.2 Cement Curing and Sample Preparation

Cement slurries were placed into sealed PVC tube molds with the dimension of 2 in inner diameter and 8 in length (Figure 3.2) and cured under constant 100 °F temperature condition for 72 hours.

Figure 3.2 PVC molds for curing cement

Tri-axial test specimens (Figure 3.3) were prepared in accordance with ASTM D 4543 standard [41] for permeability, compressive strength and Young's modulus measurements. Tri-axial test cement specimens were cut and grounded into cylinder shape with dimensions of 4 in length and 2 in diameter with the two ends grounded to within 0.001 in to ensure the two-end surfaces were flat and parallel to each other as well as perpendicular to lateral surface.

Splitting tensile test specimens (Figure 3.3) were prepared in accordance with ASTM D 3967 standard [42]. Splitting tensile test cement specimens were cut and grounded into cylinder shape with dimension of 1.5 in length and 2 in diameter with the two ends grounded to within 0.001 in to ensure the two-end surfaces were flat and parallel to each other as well as perpendicular to lateral surface.

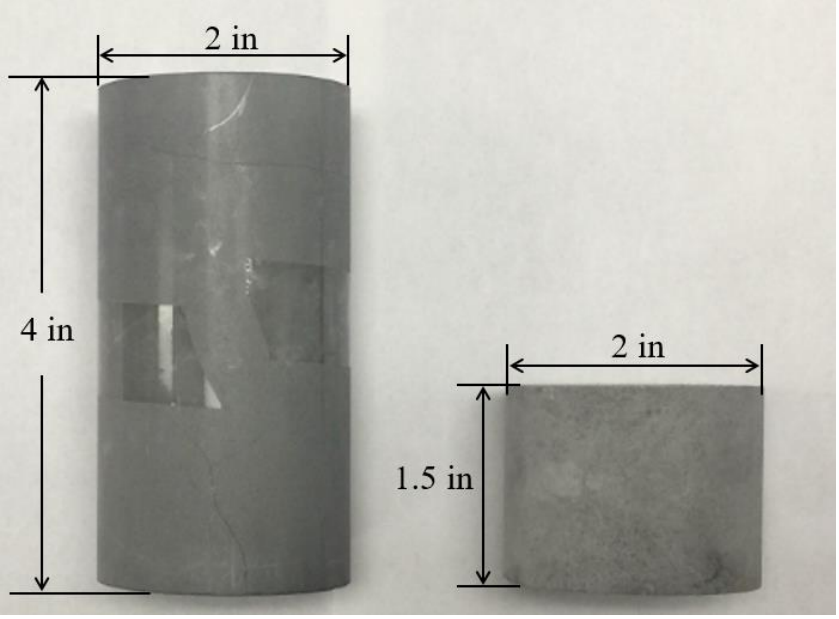

Figure 3.3 Cement specimens for tri-axial (left) and splitting tensile (right) tests

3.2.3 Cement Formulations

Cement slurries were prepared in accordance with API RP 10B-2 and API RP 10B-4 standards. As API standard recommended, a water ratio of 38 %bwoc was used, except for microsphere cement systems, which requires a large amount of water to uniformly disperse HGS. Chemical additives, i.e. dispersant, fluid loss additive and retarder, were added into different cement systems at the same concentrations. CNTs were added into different cement systems at the amount of 0.5%bwoc. Only foam cement system requires the addition of foaming agent, whose concentrations are shown in Table 3.1. HGS type 8000x was mixed into base cement slurry with the concentrations of 4.56 %bwoc and 11.95 %bwoc to lower the density to 14 ppg and 12 ppg, respectively.

The cement formulations are shown in Table 3.1.

Table 3.1 Cement formulations

Cement Type	Conv. Cement	CNT Reinforced Conv. Cement	Foam Cement		CNT Reinforced Foam Cement		Microsphere Cement		CNT Reinforced Microsphere Cement	
Water Ratio (%)	38	38	38	38	38	38	38	46	38	46
Density (ppg)	16.2	16.2	14	12	14	12	14	12	14	12
Dispersant D145A (%bwoc)	0.2	0.2	0.2	0.2	0.2	0.2	0.2	0.2	0.2	0.2
Fluid Loss Additive D193 (%bwoc)	0.15	0.15	0.15	0.15	0.15	0.15	0.15	0.15	0.15	0.15
Retarder (%bwoc)	0.1	0.1	0.1	0.1	0.1	0.1	0.1	0.1	0.1	0.1
Carbon Nanotubes (%bwoc)	0.5	0.5	0.5	0.5	0.5	0.5	0.5	0.5	0.5	0.5
Foaming Agent (%bwoc)	-	-	0.26	0.32	0.26	0.32	-	-	-	-
HGS 8000X (%bwoc)	-	-	-	-	-	-	4.56	11.95	4.56	11.95
Pre-mixing Time (s)	15	15	15	15	15	15	30	30	30	30
Pre-mixing Speed (rpm)	4000	4000	4000	4000	4000	4000	4000	4000	4000	4000
Mixing Time (s)	35 ±1	35 ±1	35 ±1	35 ±1	35 ±1	35 ±1	120 ±1	120 ±1	120 ±1	120 ±1
Mixing Speed (rpm)	12000	12000	12000	12000	12000	12000	4000	4000	4000	4000

CHAPTER 4

EXPERIMENTAL WORK

4.1 Experimental Setup

4.1.1 Cement Blender

As recommended by API Spec 10A, a two-liter, bottom-drive, blade-type, various-speed mixer was used for cement slurry preparation (Figure 4.1). The mixing blade and blender cup are constructed of durable stainless steel, which is able to withstand the corrosion caused by cement slurry and chemical additives. The bottom-drive blade can be removed for weight measurement, clean and replacement. When a 10% mass loss of blade is observed prior to mixing, a replacement of blade should be made. The mixing blade assembly is powered by a 3.5HP motor capable of up to 45000 RPM. The rotational speed is programmed at 4000 rpm and 12500 rpm (or 4000 rpm) for the two-stage cement preparation procedure. Mixing time and rotational speed are shown on the digital display.

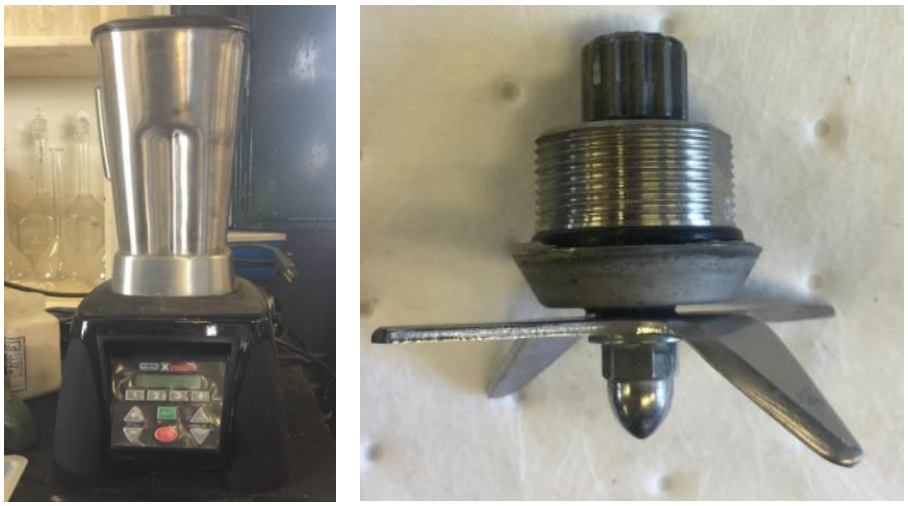

Figure 4.1 Cement blender and its blade assembly

4.1.2 Tri-axial Rock Mechanics Testing Facility

Laboratory experiments for compressive strength and Young's modulus under elevated confining pressure, and permeability measurements were conducted using Tri-axial Rock Mechanics Facility (TRMF). Figure 4.2 presents the major components of the TRMF, which includes hydraulic pump, pressure intensifiers, load frame, high-pressure cell, data acquisition system, and emergency system.

TRMF can accommodate cylindrical specimens of a length to diameter ratio of up to 3.0. In this study, a length to diameter ratio of 2.0 was used for cement specimens. The cement specimen is wrapped with a thin, deformable heat-shrink rubber, which serves as an impermeable barrier to prevent fluids contamination between pore fluid (distilled water) and confining fluid (mineral oil). Two cable ties are clamped on the top and bottom of the rubber cover to seal the test specimen. The strain measurement devices are closely attached on the specimen, which includes two axial and one circumferential strain measurement devices. Axial and circumferential strains are calculated by the measured movement over initial value. The strain measurement devices can withstand up to 200 MPa pressure and up to 150 °C temperature.

Axial stress and confining pressure can be applied on cement samples simultaneously, simulating an isotropic downhole horizontal stress condition. Axial load, confining pressure and pore pressures are powered by a hydraulic pump, which has up to 10 gpm flow rate and up to 3,000 psi pressure. The intensifiers are used to elevate the pressure transmitted form hydraulic pump to a desired value. Axial force up to 500 kN can be applied to cement sample. The Confining Pressure (CP) intensifier has a 560 cc volumetric capacity and can provide pressure up to 140 MPa (20,000 psi). The pressures at the top and bottom of test sample are powered by two independent pore pressure (PP) intensifiers, which can applied a constant pressure difference across test sample. The

real-time flow rate under a constant pressure difference can be measured. The maximum pore pressure and volumetric capacity of each PP intensifier are the same as CP intensifier.

Axial stress, axial load, confining pressure, pore pressures, volumetric flow rates, axial and circumferential strains are real-time monitored and displayed on the computer.

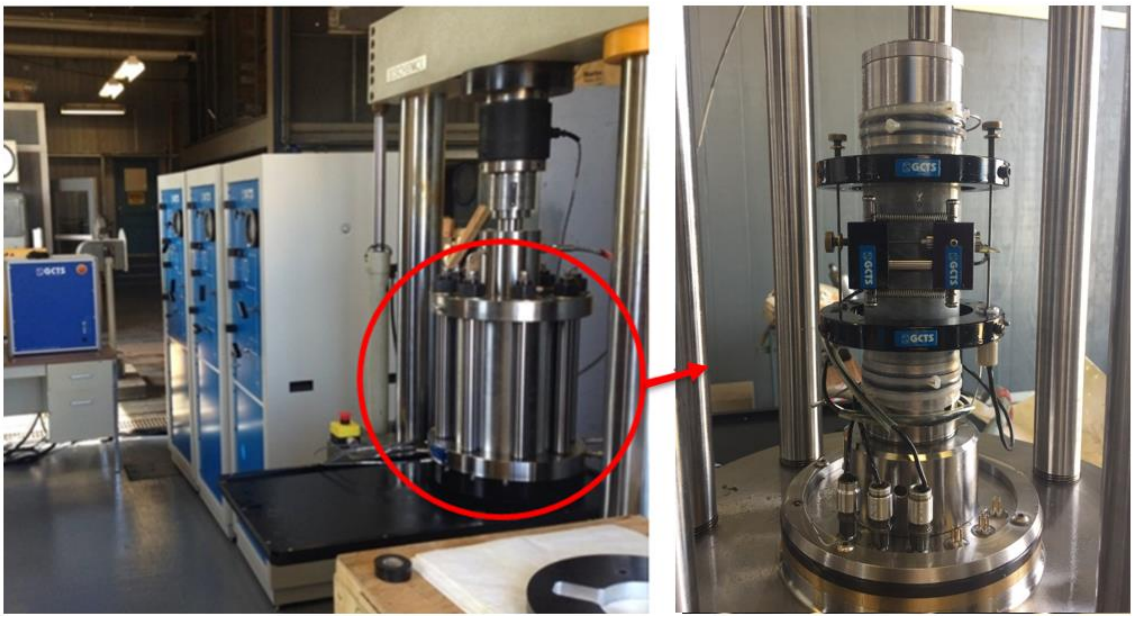

Figure 4.2 Tri-axial rock mechanics facility

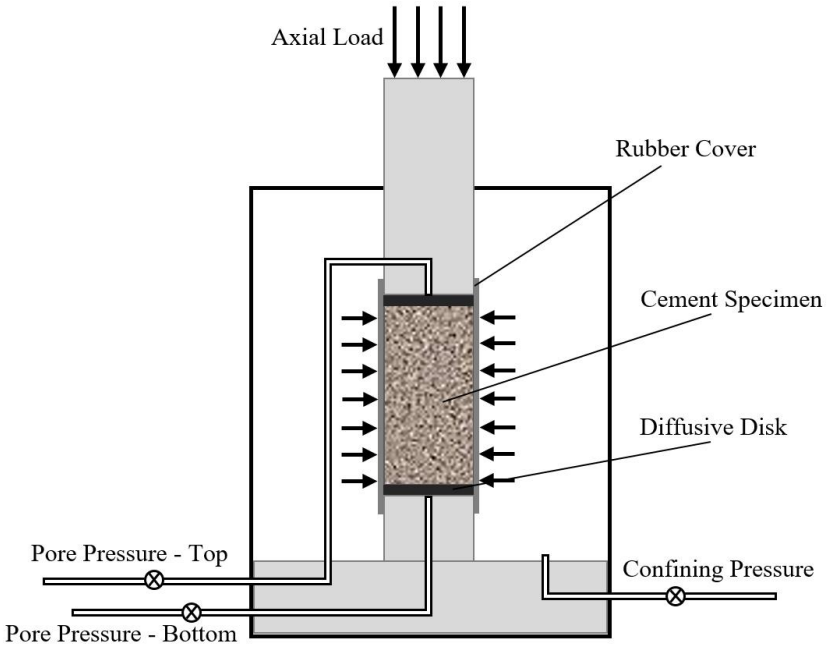

Figure 4.3 Schematic of Tri-axial rock mechanics facility

4.1.3 Splitting Tensile Test Facility

As shown in Figure 4.4, the Point Load Test Facility (PLTF) comprises a two-column fixed crosshead frame, a digital real-time force display, and a hand-operated hydraulic jack. Two aluminum false platens are used to hold samples, which enables axial load to be applied on the column lateral surface of test samples. Axial load is applied by the hydraulic jack extends the piston pushing the lower platen to move upwards. Test specimen is place in the middle of the platens. The upper platen is fixed to the crosshead with a digital display mounted on the top to provide real-time loads measurement for the calculation of splitting tensile strength. Axial loads up to 55 kN can be applied to specimens as large as 101.6 mm in diameter. The specification of PLTF are shown in Table 4.1.

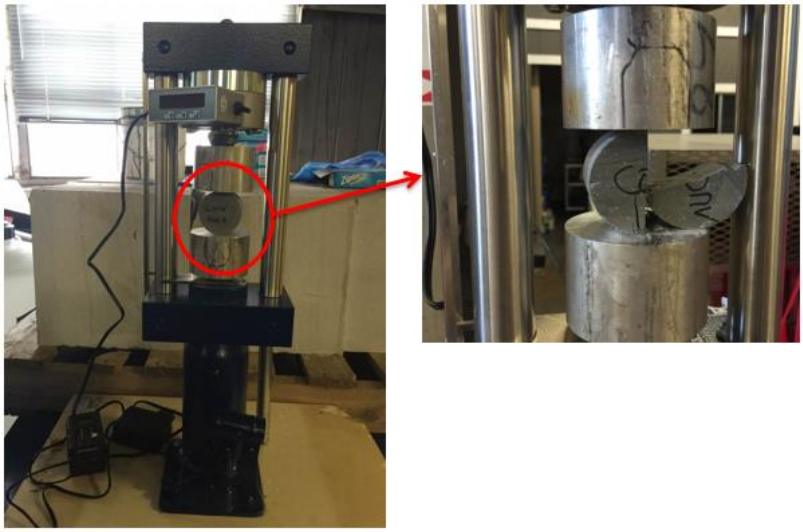

Figure 4.4 Splitting tensile test facility

Table 4.1 Specifications of Point Load Test Facility

Capacity	55kN
Maximum Sample Diameter	101.6mm
Load Range	0 to 55kN
Load Accuracy	0.001kN

4.1.4 Scanning Electron Microscope

Scanning electron microscope (SEM) is a microscope that projects electrons in a vacuum space rather than visual light to form image at micro or nano scale. The produced image is generated by collecting reflected X-rays and electrons from specimen, and converting them into digital signals. Because SEM tests are conducted under vacuum conditions and test specimens need to be mental coated, special preparations of cement specimens are required. All kinds of water in test specimen must be removed to avoid vaporization during the test. Cement specimen needs to be coated with a thin atom-layer of gold to be conductive to receive electrons. A thoroughly dehydrated condition facilitate gold atom to attach to the cement specimen.

As shown in Figure 4.5, cement specimens were prepared within 5-10mm diameter and 2-4mm thickness. The cement chips were placed in a vacuum chamber filled with argon gas. An electric field was applied in the chamber, making argon atoms to be positively charged. Positive argon ions were attracted to negatively charged gold foil. The gold atoms are knocked out from the surface of foil by argon ions, fall onto the surface of cement chips.

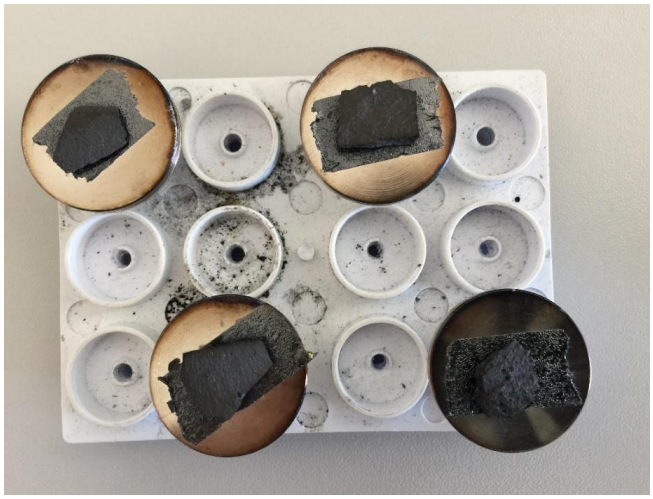

Figure 4.5 Cement chips for SEM tests

4.1.5 Rheology Test Systems

4.1.5.1 Foam Generator and Viscometer

Figure 4.6 shows foam generator and viscometer (FGV), a closed rheology test system, which enables foam cement slurry to be prepared and tested under constant system pressure. Figure 4.7 shows the schematic of FGV [43]. Conventional cement slurry is prepared and placed in the one-liter liquid bottle. Foaming agent is added into conventional cement slurry before pumping into foam generator chamber. After a fixed volume of cement slurry is pumped into mixing chamber, adjust the position of piston to control the volume of injected air by manipulating air inflow valves (i.e. V1, Pressure Regulator, V3, V4 and V5). The foam quality is defined as the total volume of air divided by the total volume of slurry. The volume of each phase is measured by the measurement tape attached on piston.

Air is blended into cement slurry by the bottom-drive blade. The foam cement slurry is prepared under constant system pressure applied by nitrogen bottle. Pressure is controlled and monitored by pressure regulator, gauges and pressure transducers on the air in flow line. As shown in Figure 4.8, three pressure transducers are connected to the air inlet, piston top, mixing chamber to monitor the pressures of air inlet, upper chamber and mixing chamber, respectively. A pressure monitoring system, programmed by LabView (Figure 4.9), was installed to collect the digital signals from pressure transducers and display the real-time pressures. When abnormal pressure is observed, slurry preparation should be stopped immediately.

After foam cement slurry is prepared, lower the piston to make slurry flow through viscometer for rheology measurement.

Figure 4.6 Foam generator and viscometer

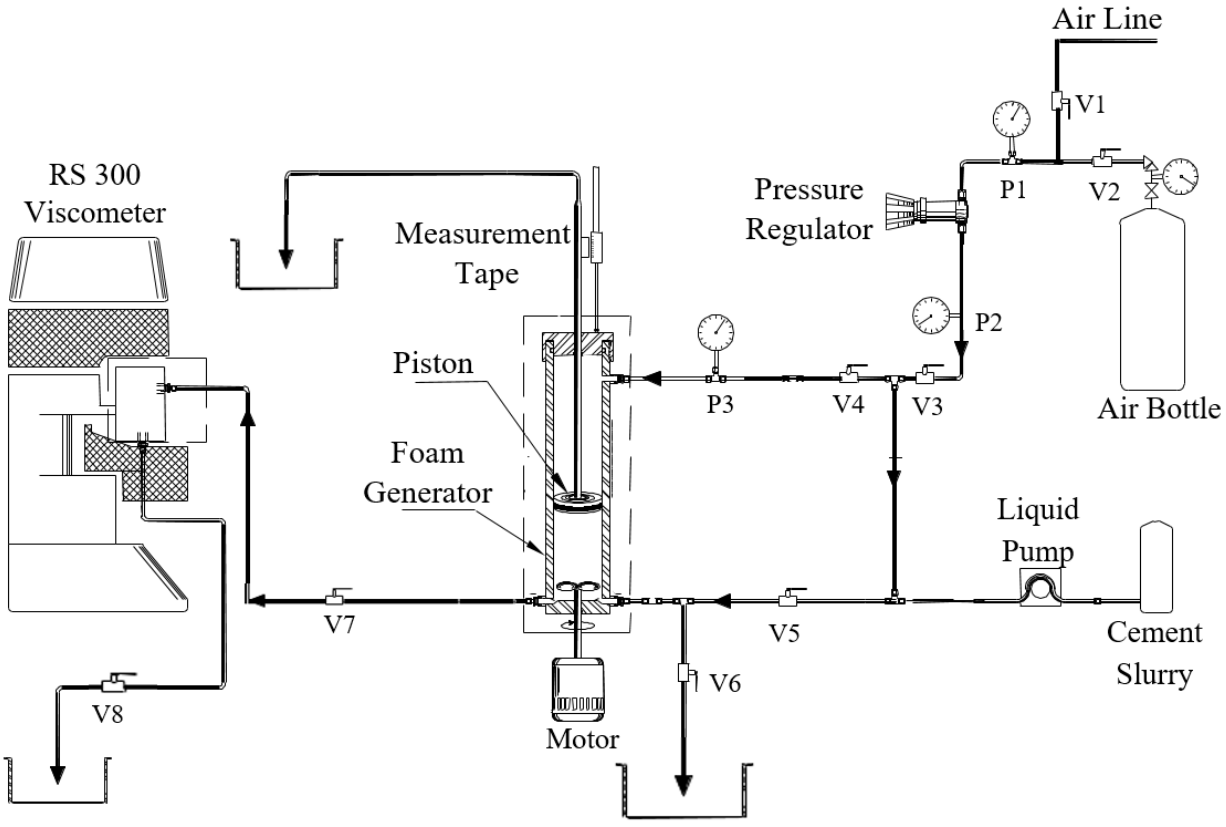

Figure 4.7 Schematic of foam generator and viscometer

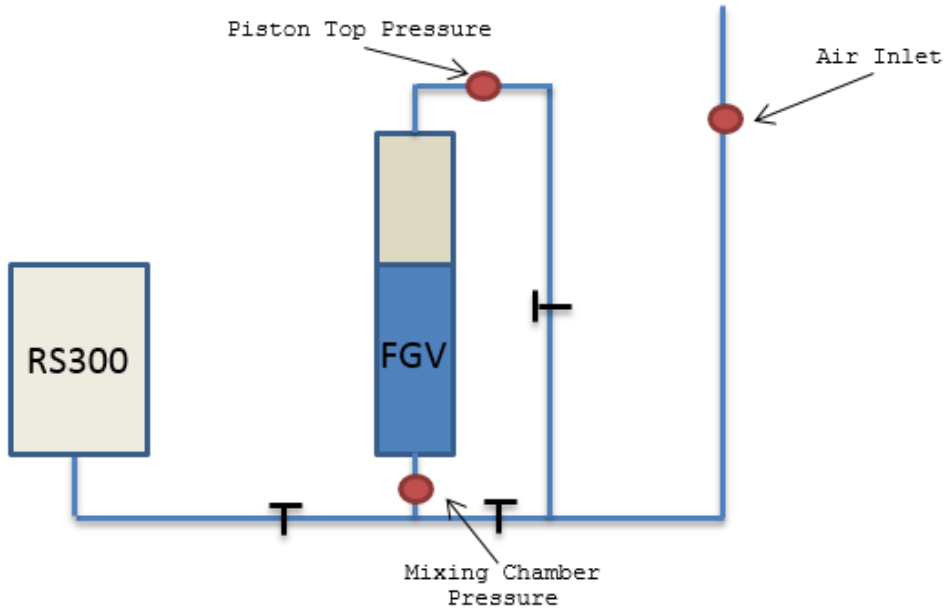

Figure 4.8 Positions of digital pressure transducers

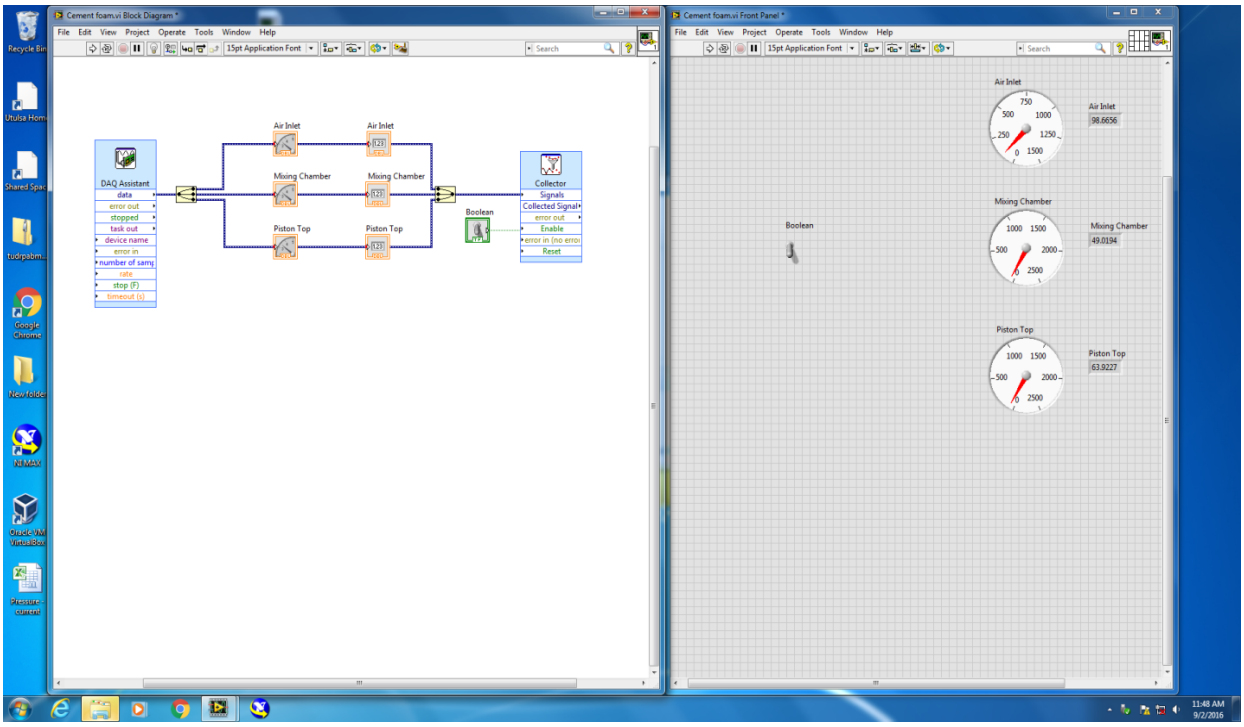

Figure 4.9 Pressure monitoring system

4.1.5.2 Modified Rheology Testing Facility

FGV can be used for the rheology measurements of foam cement slurry, conventional cement slurry and microsphere cement slurry. However, FGV requires a lot of facility cleaning time, due to its complicated pipe lines and a large number of valves and pressure gauges. The big upper part of air in foam generator chamber makes the system pressure and foam slurry outflow rate difficult to control.

A simplified rheology testing facility was designed for better system pressure control by reducing the size of pressure chamber. The reduced number of pipelines and valves enables the rheology test to be conducted in a time-saving manner. As shown in Figure 4.10, the pressure chamber comprised of a stainless steel chamber, a float piston and a removable lid connected to the viscometer. Cement slurry is prepared in cement blender in accordance with API 10B-2 before pouring into the upper part of pressure chamber. The lower part of pressure chamber is connect to air inflow line to control the system pressure. The liquid in the upper part and gas in the lower are separated by the float piston. Double O-rings are assembled on float piston to guarantee a good seal. The pressure regulator and gauges (P1 and P2) are used for adjusting and monitoring system pressure.

Figure 4.10 Modified rheology test facility

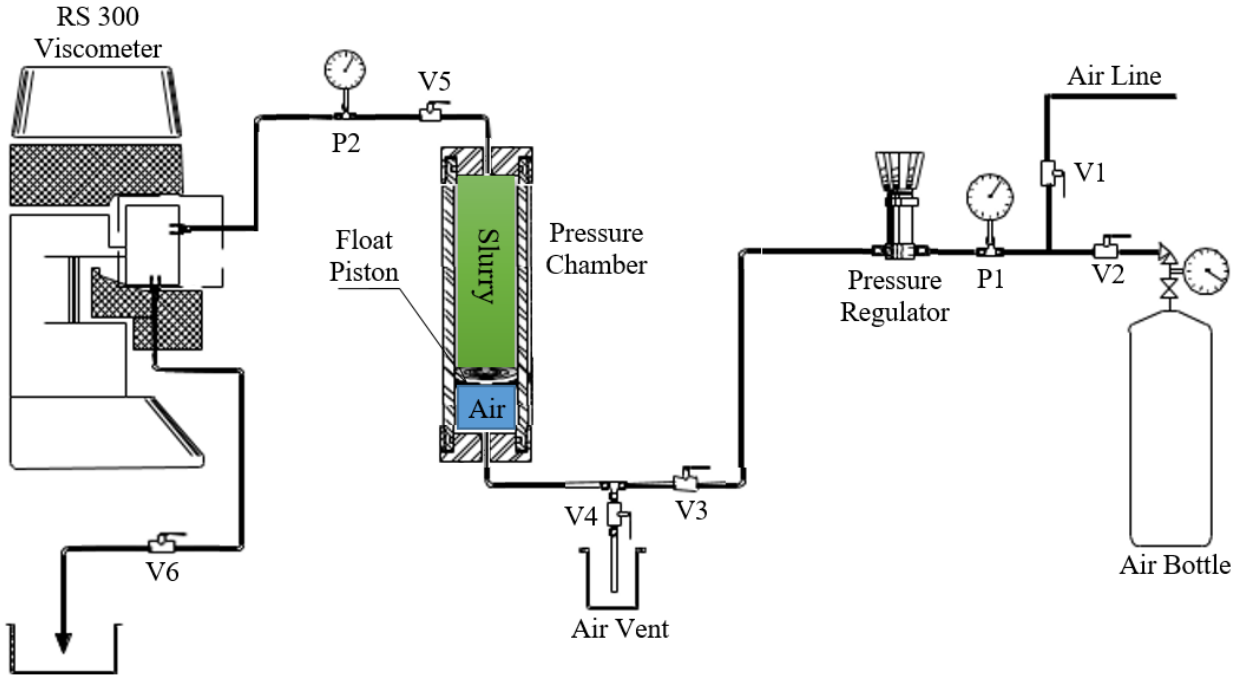

Figure 4.11 Schematic of modified rheology test facility

4.1.5.2 Flow-through Rheometer RS300

The Thermo Haake RS 300 viscometer enables cement slurry to enter at the top of the measurement cup and leave at the bottom; thus, any foam degradation during rheology measurement can be compensated by new foam cement slurry flowing into the measuring cup. The rotor is submerged in cement slurry and driven by the magnetic force applied by top motor. The rough surfaces of rotor and inner chamber reduce the wall-slip effect for accurate shear stress and viscosity results.

A data acquisition system was installed on the RS300 rheometer to record temperature, shear rate, shear stress, and viscosity.

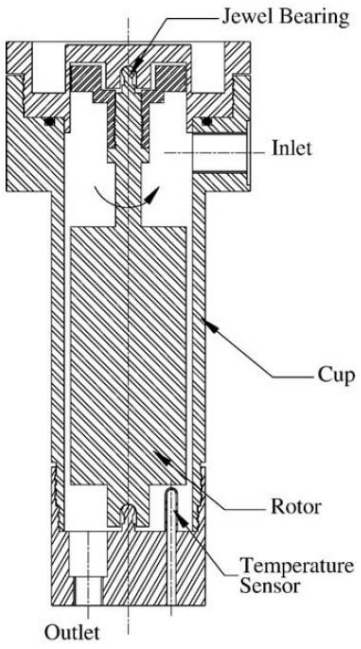

Figure 4.12 Schematic of RS300 [4]

4.2 Experimental Methods

4.2.1 Compressive Strength and Elastic Properties Tests

The mechanical properties of cement specimens (4 in. length × 2 in. diameter) were tested using the TRMF in accordance with ASTM D 7012 standard [44]. Cylindrical cement specimens were placed in tri-axial cell with axial and circumferential strain gauges (Figure 4.2). The tri-axial tests were performed with a constant strain rate of 0.012%/min (2×10^{-6}/sec) to control the axial loading rate. Compressive strength and elastic properties of cement specimens were measured under constant confining pressures of 0, 500 and 1000 psi. The confining pressure was applied isotopically on test sample, which indicates the total axial stress is the summation of applied axial stress and constant confining pressure.

During each test, an initial deviator stress of 200psi was applied on cement sample. For confined compressive strength tests, an initial confining pressure of 200psi was applied. The confining pressure was gradually increased from 200psi to 500psi in 5minutes (or 1000psi in 13 minutes) at a constant rate. The axial loading process starts when a desired confining pressure was reached. In the meanwhile, the axial and circumferential strains were measured using strain measurement, while confining pressure kept constant. The relations for the values of the Young's modulus and Poisson's ratio are expressed as:

$$E = -\frac{\sigma_a}{\varepsilon_a} \tag{4.1}$$

$$\nu = -\frac{\varepsilon_r}{\varepsilon_a} \tag{4.2}$$

There are several approaches for the calculation of Young's modulus from stress-strain plot. In this study, the average approach was used, which calculates the average slope of more or less linear part of the stress-strain plot. The compressive strength was obtained by axial loading of

the cement specimens under strain control until ultimate strength was reached. The ultimate strength is defined as the point where the slope of stress-strain plot is equal or less than zero (strain softening occurs).

4.2.2 Permeability and Porosity Tests

The permeability was calculated by applying a pressure difference across a hardened cement specimen and measuring the water inflow/outflow rates at two ends. According to the schematic shown in Figure 4.3, two pore pressure intensifiers were used to apply pressures independently at the top and the bottom surface of cement specimens. To uniformly distribute the flow of water at cement-platen interface, two 2 in diameter diffusive porous discs were placed at two ends. A confining pressure of 300psi was applied to prevent water flowing from the sample ends into tri-axial cell. When pressure difference was stabilized and inflow rate at one end was matched to outflow rate at the other end, the permeability of a cement specimen was evaluated. Flow of a Newtonian fluid through the cement specimen as a porous medium can be described by Darcy's law:

$$k = \frac{\mu Q}{A}\frac{L_t}{\Delta P} \tag{4.3}$$

A low value of permeability is an indicator of a good quality cement and ensures the zonal isolation.

Cement sample was fully hydrate by submerging in water for 10 days before conducting permeability tests. Porosity was measured by weighting the difference of cement sample before and after dehydration. We assume all void spaces, caused by initial micro cracks and pores, inside cement sample were filled with water during the 10days hydration period. The total volume of

void spaces was calculated by the weight difference divided by water density. The porosity ϕ of a cement sample is:

$$\phi = \frac{V_{void}}{V_t} \tag{4.4}$$

4.2.3 Splitting Tensile Strength Tests

Cement composite exhibits high compressive strength and low tensile strength. Downhole cement sheath encounters complicated stress conditions, including gravitational force exerted by the upper part, formation compression, casing thermal expansion, etc. When cement sheath is exposed to large internal pressure from casing, tensile failure occurs if the tension exceed its limit. Especially when conducting a hydraulic fracturing job in production casing, cement sheath cracks due to the tension applied by highly pressurized fracturing fluid.

Direct uniaxial tensile strength measurement is difficult to perform on cement specimen due to its brittle nature. In direct tensile strength tests, the cement compressive failure occurs at the two ends of a specimen caused by clamping prior to the tensile failure in the middle while applying tensile stress in axial direction. An alternative tensile strength measurement, splitting tensile strength test, also known as Brazilian test, was used to evaluate the splitting tensile strength of cement specimens. According to ASTM D 3967 standard [42], splitting tensile failure was measured by a line compressive load applied to the curved lateral surface of cylindrical specimens of 2 in diameter and 1.5 in length.

The maximum load recorded (F) is used for the calculation of splitting tensile strength T_0 of cement specimens:

$$T_o = \frac{2F_{max}}{\pi D L_s} \tag{4.5}$$

4.2.4 Brittleness Index

For evaluation of brittleness/ductility of cement sheath under downhole conditions, it is important to quantify the brittleness of cement specimen under tri-axial conditions. Consider a cement specimen loaded to the ultimate strength with a stress-strain diagram. The onset of yielding corresponds to point A and the peak strength appears at point B. The onset of fracture sliding occurs at point C. According to Hucka and Das (1974) [45], brittleness index (BI) is defined as the ratio of reversible strain energy to the total strain energy at ultimate strength:

$$\text{BI} = \frac{\text{DE}}{\text{OE}} \tag{4.6}$$

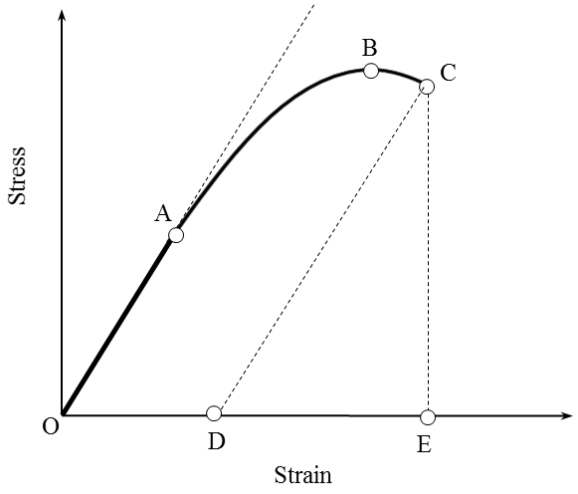

Figure 4.13 Brittleness determination from stress-strain diagram [45]

4.2.5 Unset and Set Cement Stability Tests

A standard 250-ml graduate cylinder is used for stability test of unset foam cement slurry. The top of the graduate cylinder was sealed to prevent water vaporization. The volume change of foam cement slurry was measured after a 2-hour waiting period.

8-in PVC tubes with two-end seal caps were used as curing mold. Cement slurry was cured under constant 100^{o}F temperature for 72 hours to avoid thermal shock induced stress fracturing. The set cement stability is evaluated by measuring the density of each section along the PVC tube.

Signs of unstable cement slurry are summarized below.

a) large measured density variations from top to bottom
b) visual color variation from top to bottom, which indicates the signs of density difference
c) discontinuous cement column
d) for foam cement slurry, besides the signs mentioned above, signs of large bubbles coalescence and breakout on the top surface

4.3 Test Matrix

This project consists of four stages:

The first stage is preliminary tests, which aims to validate the strengthening effect of two different nanoparticles, i.e. nano-silica and carbon nanotubes, and find the better strengthening nano-material for the following experiments.

Table 4.2 Test matrix of preliminary tests

Test Type	Cement Sample Type (material)
Uniaxial compressive strength test	Conventional cement
Uniaxial compressive strength test	Conventional cement + 0.5%bwoc Nanosilica
Uniaxial compressive strength test	Conventional cement + 0.5%bwoc Carbon Nanotubes

Preliminary test results (shown in Section 4.4) indicate that CNTs outperform nanosilica on improving cement compressive strength. Based on the uniaxial compressive strength results collected from preliminary test, the second stage test matrix was designed (Table 4.2), which uses carbon nanotubes (CNTs) as cement reinforcing material. CNTs were mixed into conventional cement slurry, microsphere cement slurry and foam cement slurry at the concentration of 0.5% bwoc. As shown in Table 4.2, 33 tri-axial tests were conducted. Lightweight cement slurries (foam and microsphere cement slurries) were prepared with the densities of 12 and 14 ppg, respectively. Water extended conventional cement with the density of 14 ppg was included in test matrix as a control group. Unset and set cement stability tests were conducted on each lightweight cement slurry system mentioned in Table 4.2. Only stabilized lightweight cements with proper densities were used for tri-axial tests.

Table 4.3 Test matrix of tri-axial tests

Tri-axial Test Conditions	Cement Type	Density (ppg)
Uniaxial Compressive Strength Test (No confining pressure)	Conventional cement	16.2
	CNT reinforced conventional cement	16.2
	Microsphere Cement	12 and 14
	CNT reinforced microsphere cement	12 and 14
	Foam cement	12 and 14
	CNT reinforced foam cement	12 and 14
	Water extended conventional cement	14
Tri-axial test under 500psi confining pressure	Conventional cement	16.2
	CNT reinforced conventional cement	16.2
	Microsphere Cement	12 and 14
	CNT reinforced microsphere cement	12 and 14
	Foam cement	12 and 14
	CNT reinforced foam cement	12 and 14
	Water extended conventional cement	14
Tri-axial test under 1000psi confining pressure	Conventional cement	16.2
	CNT reinforced conventional cement	16.2
	Microsphere Cement	12 and 14
	CNT reinforced microsphere cement	12 and 14
	Foam cement	12 and 14
	CNT reinforced foam cement	12 and 14
	Water extended conventional cement	14

Splitting tensile tests were also performed on seven different cement systems (Table 4.4), i.e. conventional cement, CNT reinforced conventional cement, microsphere cement, CNT reinforced microsphere cement, foam cement, CNT reinforced foam cement, and water extended conventional cement. The result of splitting tensile strength is the average of three repeated tests.

Table 4.4 Test matrix of splitting tensile tests

Cement Type	Density (ppg)
Conventional cement	16.2
CNT reinforced conventional cement	16.2
Microsphere Cement	12 and 14
CNT reinforced microsphere cement	12 and 14
Foam cement	12 and 14
CNT reinforced foam cement	12 and 14
Water extended conventional cement	14

Third stage experiments utilized scanning electron microscope to analyze CNTs bridging and reinforcing effects, foam and microsphere dispersion in cement composite, and structural difference among different cement systems.

Fourth stage is cement rheology tests (Table 4.5).

Table 4.4 Test matrix of rheology tests

Cement Type	Density (ppg)	Pressure	Temperature
Conventional cement	16.2	Ambient	20°C
CNT reinforced conventional cement	16.2	Ambient	20°C
Microsphere Cement	12	Ambient	20°C
	14	Ambient	20°C
CNT reinforced microsphere cement	12	Ambient	20°C
	14	Ambient	20°C
Foam cement	12	Ambient and 500psi	20°C
	14	Ambient and 500psi	20°C
CNT reinforced foam cement	12	Ambient and 500psi	20°C
	14	Ambient and 500psi	20°C
Water extended conventional cement	14	Ambient	20°C

4.4 Preliminary Test Result

Preliminary tests consist of uniaxial compressive strength tests and rheology tests of conventional cement, nano-silica reinforced cement and CNTs reinforced cement. Nano-silica and multi-walled carbon nanotubes were mixed into conventional cement slurry at the concentration of 0.5 % bwoc. Test result are shown in Figure 4.14 and Figure 4.15.

As shown in Figure 4.14, CNTs outperform nano-silica on enhancing compressive strength of cement composite. Moreover, as shown in Figure 4.15, the addition of 0.5 % bwoc nano-silica significantly increased the viscosity of cement slurry, resulting in an unpumpable fluid. By contrast, the addition of 0.5 % bwoc CNTs exhibits negligible viscosity change.

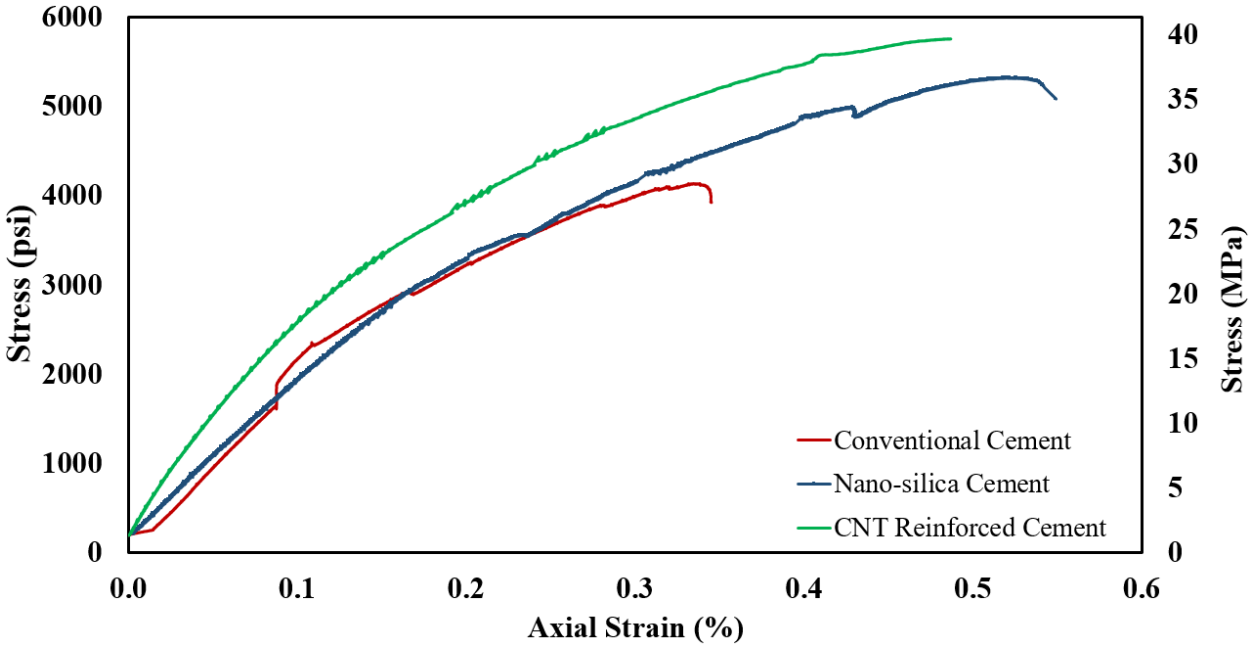

Figure 4.14 Preliminary tests result of uniaxial compressive strength

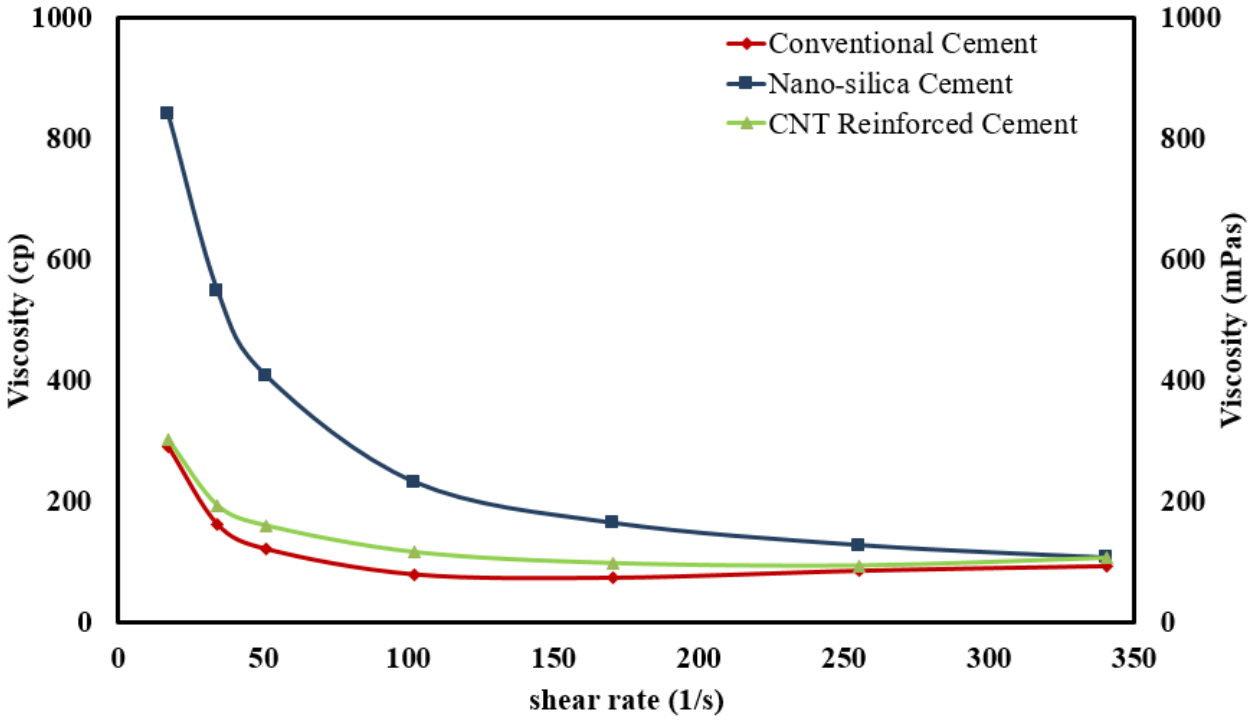

Figure 4.15 Preliminary tests result of cement rheology

CHAPTER 5

RESULTS AND DISCUSSIONS

5.1 Mechanical Properties

5.1.1 Stress-strain Plots of Tri-axial Experiments

An example of stress-strain plot for CNT-reinforced microsphere cement specimen under different confining pressures is given in Figure 5.1. The tests have been conducted according to a strain control mechanism. As shown in Figure 5.1**,** the compressive strength increases with increasing confining pressure. The initial part of the plots show a linear trend between the stress and strain, which is used for the calculations of Young's modulus. At low confining pressures of 0 and 500 psi, the behavior of cement specimens at failure was followed by a sudden reduction in the axial stress with further straining. At a higher confining pressure of 1000 psi, the cement specimen was able to carry larger axial loads without sudden reductions. Instead, cement specimen kept deforming with little stress increment. The axial load continues to increase until the slope of the axial stress-strain plot approaches to small values close to zero. Moreover, the lateral to axial strain ratio is less than 0.1, which reveals a high degree of incompressibility of the cement specimens in the lateral direction (low Poisson's ratios).

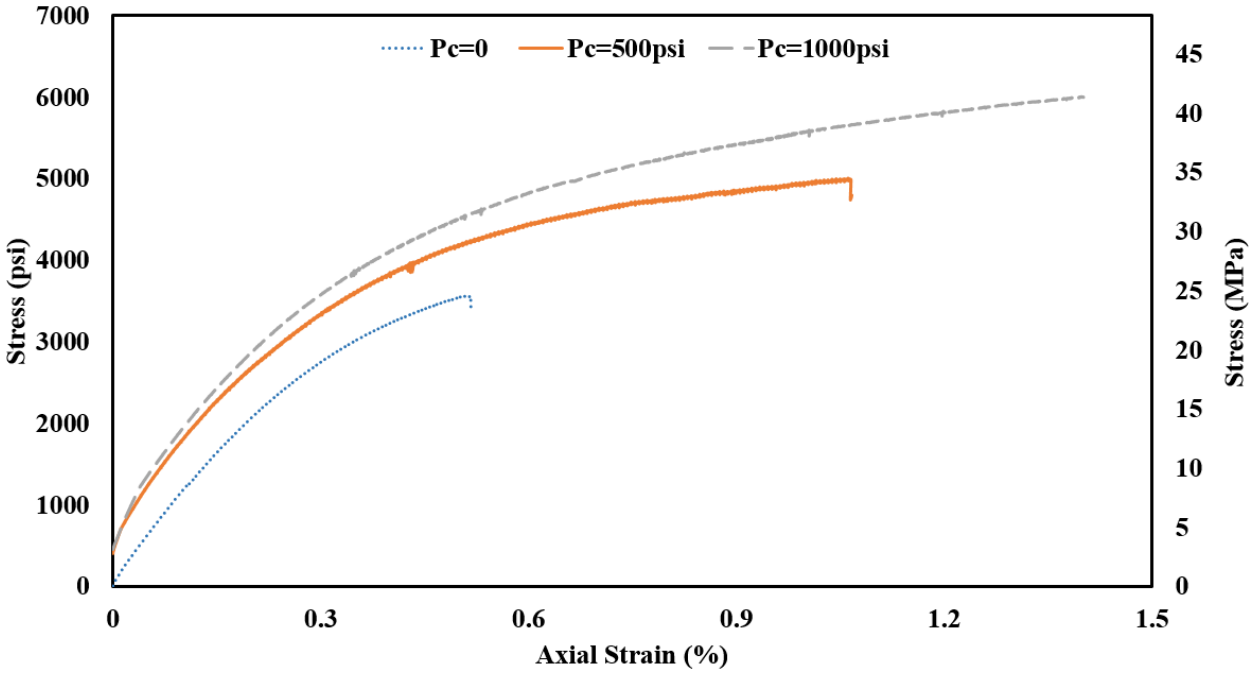

Figure 5.1 Stress-strain plot for CNT-reinforced microsphere cement

5.1.2 Young's Modulus

Figure 5.2 illustrates the bar graph representation of Young's modulus of various cement systems, namely, conventional cement, water-extended cement, foam cement, microsphere cement, and their CNT-reinforced compartments. Young's modulus was estimated from the initial linear part of the stress-strain plot using the average approach.

For all of the cement systems, the Young's modulus shows an increasing trend with confining pressure, except for the water extended cement. However, the amount of increase in Young's modulus with increasing confining pressure is not significant, compared to other influence factors. This is because of the fact that the hardened cements are isotropic medium with low porosity and Poisson's ratio. Moreover, Young's modulus of conventional cement specimen is larger than that of the other cement systems. Another observation is that the addition of CNTs

lowers the Young's modulus of conventional cement specimens, while the addition of CNTs shows negligible effect in Young's modulus of lightweight cement systems.

Compared to the air-solid structure of foam and microsphere cements, conventional cement has single solid phase with low compressibility, which is unable to store as much deformation as air bubbles. When subjected to the same value of compressive stress, the lightweight cements exhibit more deformation and compressibility due to the compressed air bubbles in cement composite, resulting in a lower Young's modulus.

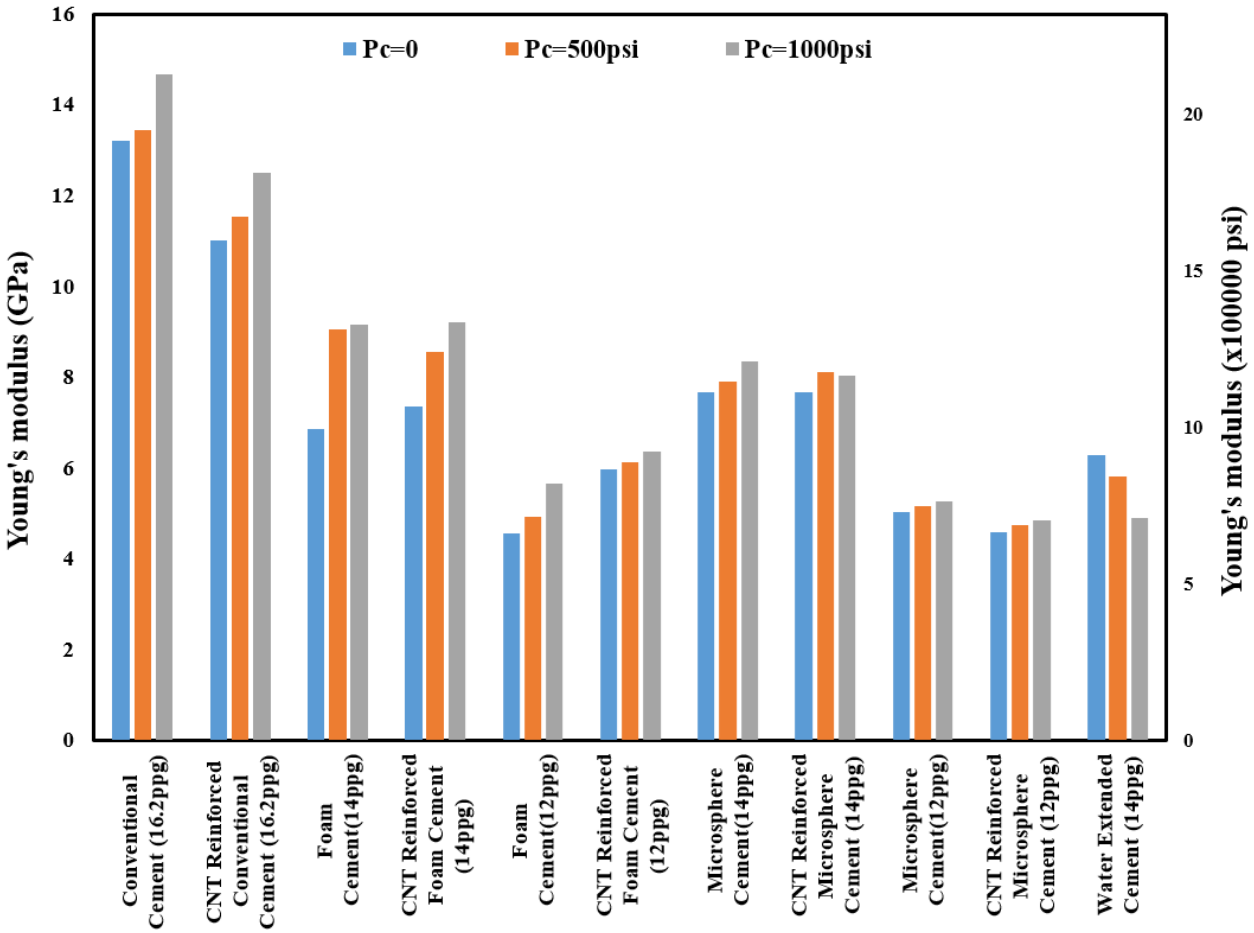

Figure 5.2 Young's modulus of various cement systems under tri-axial conditions

Figure 5.3 presents the Young's modulus of microsphere and foam cements with the densities of 12 ppg and 14 ppg under different confining pressures. As shown in Figure 5.3, Young's modulus increases with cement density and confining pressure. However, the effect of

confining pressure on Young's modulus is negligible, compared to that of cement density. Foam and microsphere cement systems with the same density exhibit similar values of Young's modulus. Thus, Young's modulus of lightweight cement is strongly affected by cement density, instead of lightweight techniques or confining pressure.

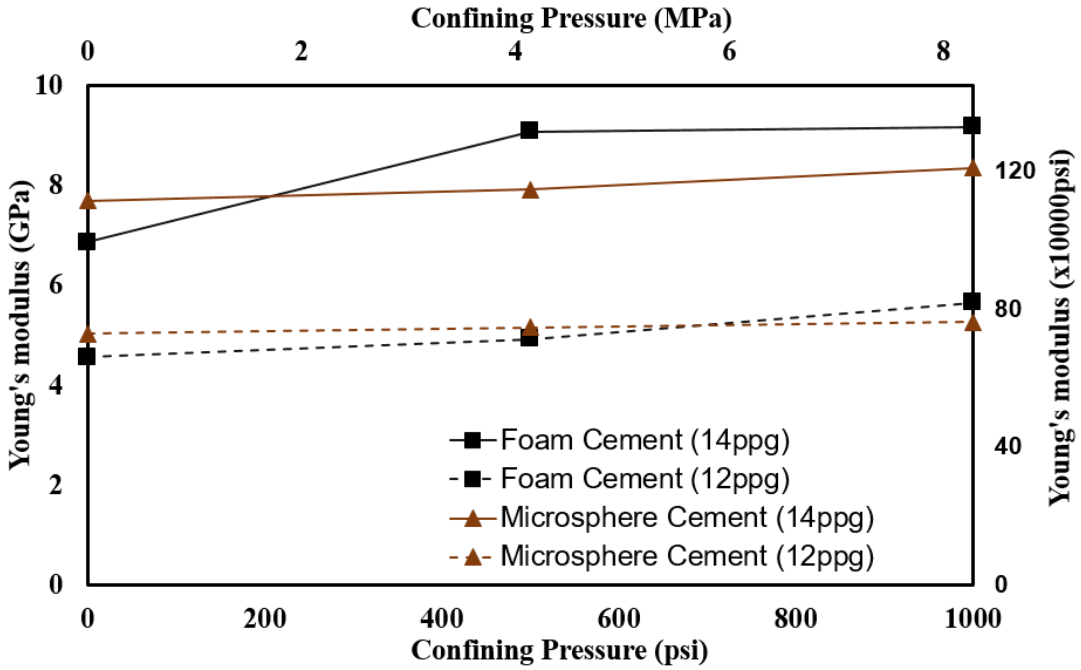

Figure 5.3 Young's modulus of foam and microsphere cements under tri-axial conditions

5.1.3 Compressive Strength

The compressive strength for various cement systems as a function of confining pressure is depicted in Figure 5.4. From this figure, the compressive strength increases with increasing confining pressure from 0 to 1000 psi. The compressive strength of conventional cement is higher than that of other lightweight cement systems. For instance, the conventional cement under uniaxial loading is able to withstand 4140 psi axial stress, while the foam cement, microsphere cement, and water extended cement with the density of 14 ppg carry 2054 psi, 2443 psi, and 1870 psi, respectively.

As shown in Figure 5.4, water extend cement gives little stress satisfaction. The 14 ppg water extended cement shows low compressive strength due to its highest water ratio. The compressive strength of 14 ppg water extended cement is similar to that of 12 ppg foam and microsphere cements. This is most likely because increased water ratio results in a diluted cement composite, which is more susceptible to shrinkage during cement curing period. Shrinkage creates cement intrinsic micro-cracks, resulting in a weak and fragile cement system. Moreover, excessive water will create a free-liquid layer on the top of cement slurry due to the weight of aggregate and cement composite. While water is being squeezed from slurry to top surface, the paths that water flow through leaves micro channels that provide a passages for hydrocarbons and deteriorate cement overall zonal isolation.

Results also show that adding CNTs to all cement systems improves the compressive strength from 8.5% to 30%. The largest increase in compressive strength was observed for the case of unconfined compressive strength. It should be noted that intrinsic cement micro-cracks and pores are easily to become interconnected without the presence of confining pressure. Thus, uniaxial compressive strength is not a good representation of cement strength. The strength enhancement of CNTs in cement composites can be interpreted by CNT bridging in micro cracks, as shown in Chapter 5.2.2. The ordering for compressive strength for both CNT-free and CNT-reinforced cements can be summarized as: conventional cement>microsphere cement>foam cement> water extended cement.

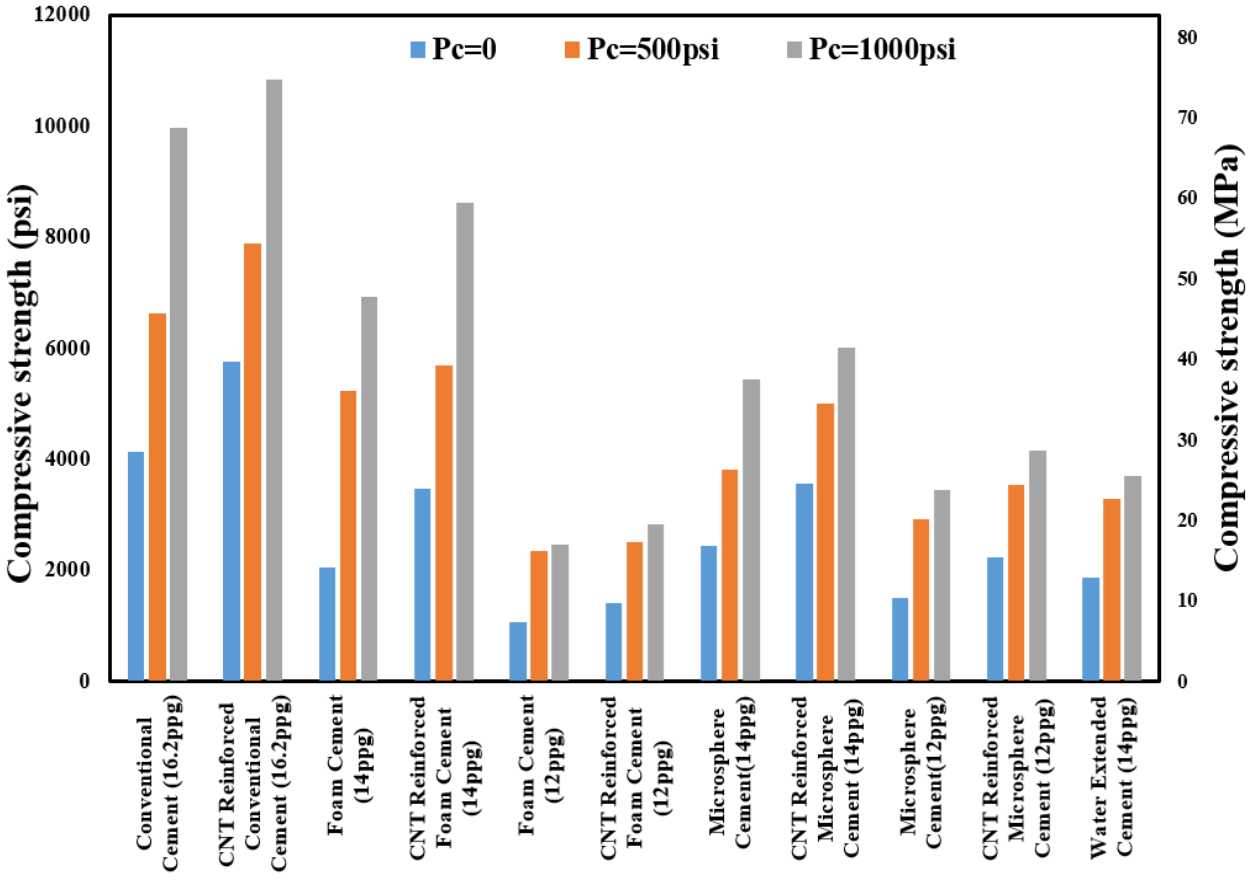

Figure 5.4 Compressive strength of various cement systems under tri-axial conditions

Besides the water ratio, another important factor that significantly decreases the compressive strength of lightweight cement systems is cement density. The compressive strength of foam and microsphere cements with different densities under confining pressures are shown in Figure 5.5. Conventional cement is the base phase of lightweight cements. Thus, conventional cement can be regarded as foam and microsphere cements with the density of 16.2 ppg. By adding foams and microspheres, the density of conventional cement decreases.

As it is discussed above, uniaxial compressive strength test is not a good indication for cement compressive strength, because unconfined test condition cannot stop intrinsic micro-cracks from extension. Compressive strength tests of lightweight cements under the confining pressures of 500 psi and 1000 psi are used for the following analysis. When slurry density was lowered to

14 ppg, foam cement exhibits higher compressive strength than that of microsphere cement. However, when the density kept decreasing to 12 ppg, microsphere cement outperforms foam cement in compressive strength.

The reason why the compressive strength of foam cement dropped more rapidly than microsphere cement as density goes lower can be interpreted by the stability of air bubbles and microspheres. The stability of air bubbles is greatly affected by temperature and pressure. Air bubbles have tendency to aggregate, merge, coalescence and rise up in cement slurry, especially when the temperature increases. As shown in Chapter 5.2.1, compared to 14 ppg foam cement slurry, 12 ppg foam cement slurry contains a larger amount of air bubbles, which makes slurry less stable. Foam coalescence is more common in low density foam cement slurry due to the increased amount of air bubbles. Such air spaces lead to higher stress concentrations when an axial load is applied, resulting in lower strength property. While microsphere cement slurry can be considered as a stable cementing fluid, unless pressure condition surpass the crush resistance of hollow glass spheres. In this study, hollow glass spheres with the crush resistance of 8000psi were used, which is way much higher than slurry curing pressure and confining pressure. That is, the stability of microsphere cement slurry do not have to be addressed. By the time microsphere cement slurry is hardened, hollow glass spheres are embedded into cement composite.

As shown in Chapter 5.2.1, the structural difference between 12 ppg and 14 ppg microsphere cements is the concentration of hollow glass spheres. A possible reason for compressive strength reduction is low density microsphere cement slurry requires a higher water ratio to disperse glass spheres. Since water ratio is a major factor that determines compressive strength, a lower strength was observed for 12 ppg microsphere cement.

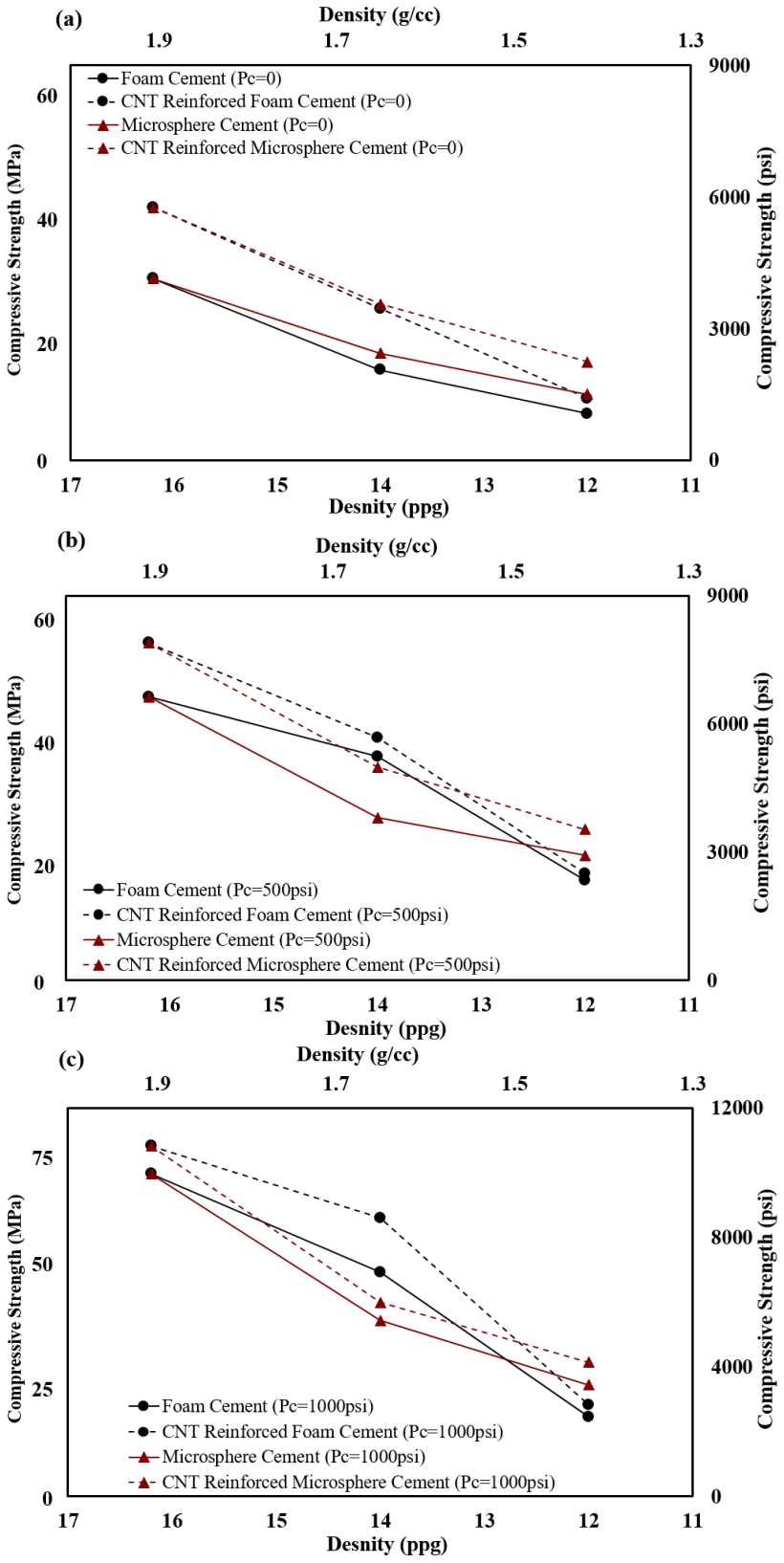

Figure 5.5 Compressive strength of lightweight cements under the confining pressures of (a) 0, (b) 500psi, and (c) 1000psi

5.1.4 Failure Criteria

Figure 5.7 shows several images of the failed cement samples after tri-axial tests. It can be seen that the induced fractures resulting from the compressive loading of cement samples are vertically-oriented. As proposed by Zaitsev and Wittmann (1981) [46], cement composite contains a lot of randomly distributed micro pores and intrinsic cracks, where initial stress are generated. When axial load is evenly applied on the cross section, these intrinsic cracks have tendency to elongate and interconnect due to stress concentration. A major crack, leading to cement failure, is generated by the extension and accumulation of micro cracks.

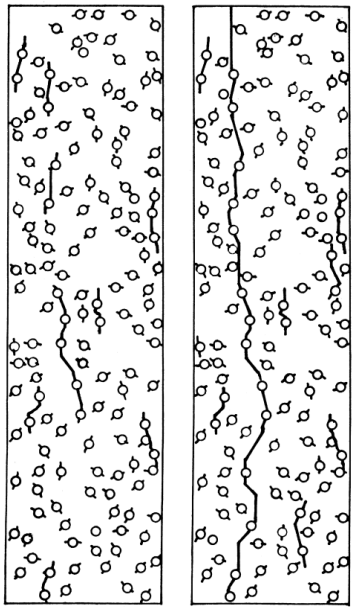

Figure 5.6 Cement composite with randomly distributed intrinsic micro cracks and pores: initial and elevated axial load conditions [46]

Figure 5.7 Cement specimens at failure

Different failure criteria were considered to evaluate cement failure. The purpose is to find an empirical failure criteria that fits experiment data and is able to describe cement failure mechanism.

Different failure criteria were evaluated by the methods of R-squared and root-mean-squared error (RMSE). R-squared value is a statistical measurement to describe how close the model predication is to the measured data. R-squared, also known as the coefficient of

determination, is in the range from 0 to1. A high R-squared value (close to 1) indicates an accurate predication.

$$R^2 = \frac{\sum_{i=1}^{N} {x_i}^2}{\sum_{i=1}^{N} {x_i}^2 - \sum_{i=1}^{N} (x_i - X_i)^2} \quad (5.1)$$

Root- mean-squared error (RMSE) is a mathematical measurement of the difference between measured data and model prediction. A low value of RMSE indicates a better model predication.

$$RMSE = \left(\frac{1}{N} \sum_{i=1}^{N} (y_i - Y_i)^2 \right)^{0.5} \quad (5.2)$$

5.1.4.1 Mohr-Coulomb Failure Criterion:

The most widely used Mohr-Coulomb failure criterion [47] assumes that cement failure is caused by normal stress σ and shear stress τ on failure plane. Axial load (normal force) results in the movement and interaction of solid particles in cement samples. Movement of solid particles along failure plane inside cement samples are restricted by a friction force, which equals the normal force multiplies a constant μ that known as a coefficient of friction.

$$|\tau| = S_0 + \mu\sigma \quad (5.3)$$

The Mohr-Coulomb criterion defines a linear relationship of $\sigma - \tau$ that intercepts the τ–axis at S_0, with a slope μ.

The angle φ is called the angle of internal friction (or friction angle), whose tangential value equals the coefficient of internal friction μ:

$$tan\varphi = \mu \tag{5.4}$$

The shear stress and normal stress on the failure plane are

$$|\tau| = \frac{1}{2}(\sigma_1 - \sigma_3)sin2\beta \tag{5.5}$$

$$\sigma = \frac{1}{2}(\sigma_1 + \sigma_3) + \frac{1}{2}(\sigma_1 - \sigma_3)cos2\beta \tag{5.6}$$

The relation of β and φ are related as follows

$$\varphi + \frac{\pi}{2} = 2\beta, \tag{5.7}$$

where β is the angle for which the failure criterion is fulfilled, and it gives the orientation of the failure plane.

By substituting Eq. (5.5) and Eq. (5.6) into the failure criterion

$$\sigma_1 = 2S_0 \frac{cos\varphi}{1 - sin\varphi} + \sigma_3 \frac{1 + sin\varphi}{1 - sin\varphi} \tag{5.8}$$

The Mohr-Coulomb failure criterion shows a linear relationship between axial stress σ_1 and confining pressure σ_3.

An observation is that cement fractures do not have a frictional nature. Therefore, the empirical models such as Mohr-Coulomb criterion, which requires measured friction angle for stress calculation, shall not be used as a failure criterion for the estimation of cement strength under tri-axial loading conditions.

5.1.4.2 Drucker-Prager Criterion:

Drucker-Prager failure criterion [48] gives a linear relationship between axial stress and confining pressure, which is the same as Mohr-Coulomb failure criterion. It can be expressed as:

$$\sqrt{J_2} = \lambda I_1' + \kappa, \tag{5.9}$$

where λ and κ depend on the properties of materials, known as material constants.

I_1' and J_2 are the first invariant of the stress tensor and the second invariant of stress deviator tensor, respectively.

$$I_1' = \sigma_1 + \sigma_2 + \sigma_3 \tag{5.10}$$

$$J_2 = \frac{1}{6}[(\sigma_1 - \sigma_2)^2 + (\sigma_2 - \sigma_3)^2 + (\sigma_3 - \sigma_1)^2] \tag{5.11}$$

where σ_1, σ_2, and σ_3 are the principal effective stresses.

Give the tri-axial rock mechanics test facility only provides constant confining pressure in radial direction,

$$\sigma_2 = \sigma_3 \tag{5.12}$$

Eq. (5.10) and Eq. (5.11) can be simplified as

$$I_1' = \sigma_1 + 2\sigma_2 \tag{5.13}$$

$$J_2 = \frac{1}{2}(\sigma_1 - \sigma_2)^2 \tag{5.14}$$

therefore,

$$\sigma_1 = \frac{\frac{\sqrt{3}}{3} + 2\lambda}{\frac{\sqrt{3}}{3} - \lambda}\,\sigma_2 + \frac{\kappa}{\frac{\sqrt{3}}{3} - \lambda} \tag{5.15}$$

As shown in Figure 5.8, the relationship of axial stress σ_1 and confining pressure σ_3 for conventional, foam, microsphere cement systems can be regarded as linear. A linear function is shown for each $\sigma_1 \sim \sigma_3$ plot. Material constants, λ and κ, were evaluated based on the linear functions. The data of material constants, R-squared and RMSE are presented in Table 5.1. The R-squared value of each $\sigma_1 \sim \sigma_3$ plot is greater than 0.9, which indicates an accurate linear prediction.

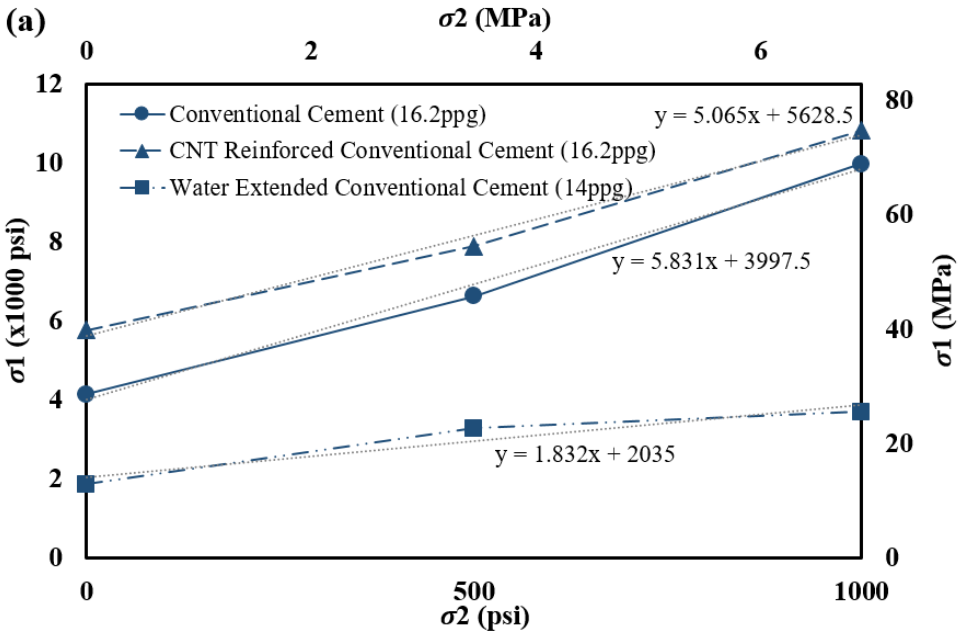

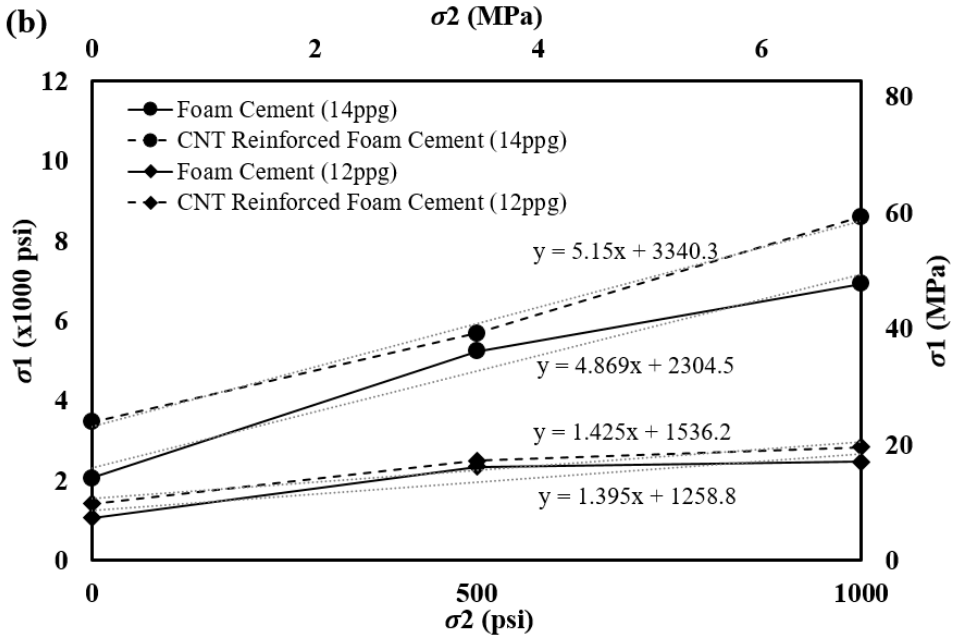

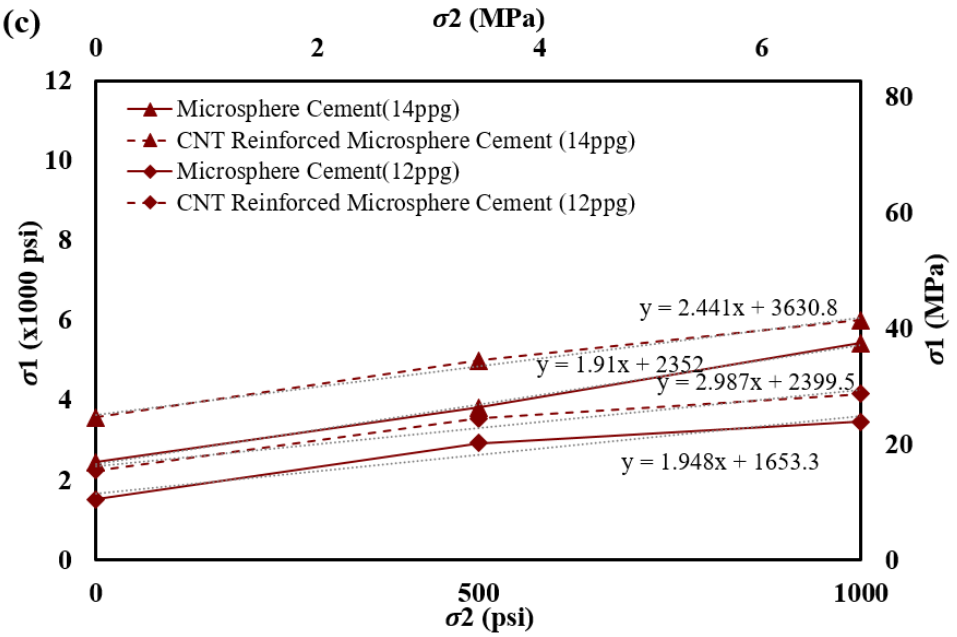

Figure 5.8 The relationship of axial stress and confining pressure of (a) conventional cement systems, (b) foam cement systems, and (c) microsphere cement systems under tri-axial conditions

Table 5.1 The Application of Drucker-Prager Failure Criterion on Different Cement Systems

Cement Sample Type (material)	Density (ppg)	Material constant λ	Material constant κ	R^2	RMSE
Conventional cement	16.2	0.356	884.162	0.9929	201.53
CNT reinforced conventional cement	16.2	0.332	1379.879	0.9916	190.21
Foam cement	14	0.325	581.091	0.9702	348.60
CNT reinforced Foam cement	14	0.335	809.171	0.9938	166.41
Foam cement	12	0.067	642.211	0.815	271.29
CNT reinforced Foam cement	12	0.072	776.869	0.9165	175.60
Microsphere Cement	14	0.230	833.378	0.9975	61.52
CNT reinforced foam cement	14	0.187	1416.062	0.9905	97.35
Microsphere Cement	12	0.139	725.329	0.9366	206.95
CNT reinforced foam cement	12	0.134	1041.888	0.9604	158.39
Water extended conventional cement	14	0.125	919.813	0.9113	233.35

5.1.4.3 Mogi-Coulomb Failure Criterion:

Mogi-Coulomb failure criterion [49] assumes shear failure occurs, when shear stress equals or greater than the summation of natural cohesion and frictional force on failure plane. This failure criterion defines a linear relationship of mean normal stress, $\sigma_{m,2}$, and octahedral shear stress, τ_{oct}:

$$\tau_{oct} = a + b\sigma_{m,2} \tag{5.16}$$

$$\tau_{oct} = \frac{1}{3}\sqrt{(\sigma_1 - \sigma_2)^2 + (\sigma_2 - \sigma_3)^2 + (\sigma_3 - \sigma_1)^2} \tag{5.17}$$

For the case of $\sigma_2 = \sigma_3$,

$$\tau_{oct} = \frac{\sqrt{2}}{3}(\sigma_1 - \sigma_2) \tag{5.18}$$

$$\sigma_{m,2} = \frac{\sigma_1 + \sigma_2}{2} \tag{5.19}$$

therefore,

$$\sigma_1 = \frac{6\ a}{2\sqrt{2} - 3\ b} + \frac{2\sqrt{2} + 3\ b}{2\sqrt{2} - 3\ b}\sigma_2 \tag{5.20}$$

The Mogi-coulomb failure criterion gives a linear relationship between axial stress σ_1 and confining pressure σ_3. The parameters, a and b, are calculated according to the linear functions given in Figure 5.8. Since Drucker-Prager and Mogi-Coulomb failure criterion used the same linear functions for rock parameters calculations, the R-squared value and RMSE are the same.

Table 5.2 The Application of Mogi-Coulomb Failure Criterion on Different Cement Systems

Cement Sample Type (material)	Density (ppg)	Parameter a	Parameter b	R^2	RMSE
Conventional cement	16.2	551.732	0.667	0.9929	201.53
CNT reinforced conventional cement	16.2	874.955	0.632	0.9916	190.21
Foam cement	14	370.200	0.622	0.9702	348.60
CNT reinforced Foam cement	14	512.076	0.636	0.9938	166.41
Foam cement	12	495.536	0.155	0.815	271.29
CNT reinforced Foam cement	12	597.255	0.165	0.9165	175.60
Microsphere Cement	14	567.412	0.470	0.9975	61.52
CNT reinforced foam cement	14	994.813	0.395	0.9905	97.35
Microsphere Cement	12	528.747	0.303	0.9366	206.95
CNT reinforced foam cement	12	762.023	0.295	0.9604	158.39
Water extended conventional cement	14	677.478	0.277	0.9113	233.35

5.1.4.4 Hoek-Brown Failure Criterion:

Hoek-Brown failure criterion [50] is defined by the equation

$$\sigma_1 = \sigma_3 + \sigma_{ci}\left(m\frac{\sigma_3}{\sigma_{ci}} + s\right)^{0.5}, \tag{5.21}$$

where σ_1 and σ_3 are the major and minor effective principal stresses at failure, σ_{ci} is the uniaxial compressive strength (UCS) of intact rock material, m and s are material constants, where $s = 1$for intact rock.

Material constant,

$$m = \left(\frac{\sigma_3}{\sigma_{ci}}\right)^{-1}\left[\left(\frac{\sigma_1 - \sigma_3}{\sigma_{ci}}\right)^2 - 1\right] \tag{5.22}$$

The data of material constants and RMSE are presented in Table 5.3.

Table5.3 The Application of Hoek-Brown Failure Criterion on Different Cement Systems

Cement Sample Type (material)	Density (ppg)	UCS σ_{ci} (psi)	material constant m	RMSE
Conventional cement	16.2	4140	15.30	858.36
CNT reinforced conventional cement	16.2	5763	11.00	664.11
Foam cement	14	2058	15.01	295.52
CNT reinforced Foam cement	14	3458	13.28	729.29
Foam cement	12	1067	0.94	560.17
CNT reinforced Foam cement	12	1412	0.98	358.66
Microsphere Cement	14	2443	5.59	271.23
CNT reinforced foam cement	14	3562	3.46	146.31
Microsphere Cement	12	1507	2.49	383.08
CNT reinforced foam cement	12	2240	2.19	297.86
Water extended conventional cement	14	1870	2.03	457.46

5.1.4.5 Haimson-Chang Failure Criterion:

Haimson-Chang Failure Criterion [51] gives a power relationship between mean normal stress $\sigma_{m,2}$ and octahedral shear stress τ_{oct} on the failure plane:

$$\tau_{oct} = A\,\sigma_{m,2}^{n}\,, \qquad (5.23)$$

where A and n are material constant.

The equations of mean normal stress, $\sigma_{m,2}$, and octahedral shear stress, τ_{oct}, are in the same form as the Mogi-Coulomb failure criterion.

Figure 5.9 shows the relationship between mean normal stress $\sigma_{m,2}$ and octahedral shear stress τ_{oct}. Material constants, A and n, were evaluated from the trend-line functions. The R-squared value of all trend-line functions are in the range of 0.9 - 1.0, except for the case of 12 ppg foam cement. That is, the Haimson-Chang Failure criterion is suitable for the simulation of conventional and microsphere cements, and may not be applied to foam cement composite.

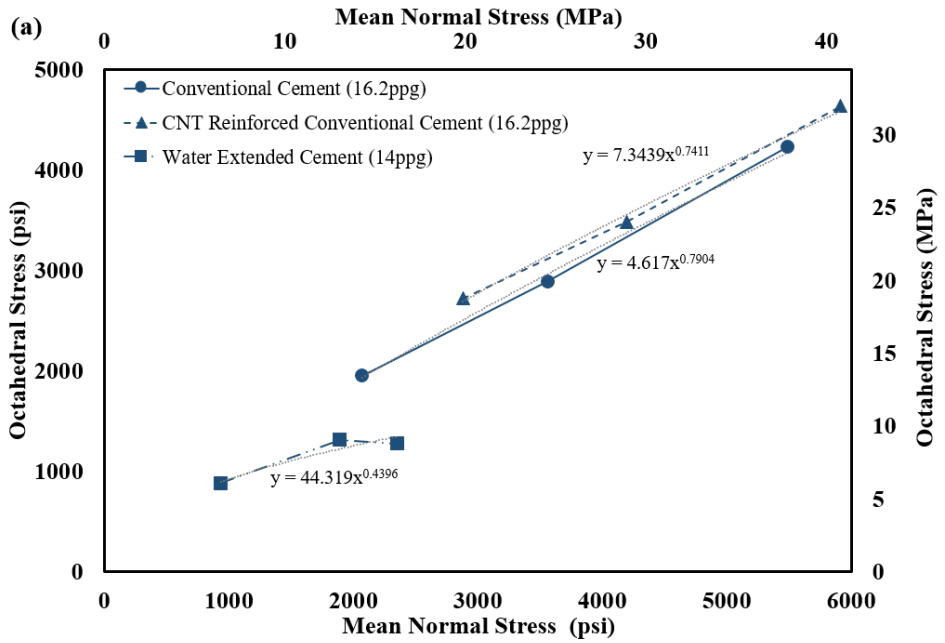

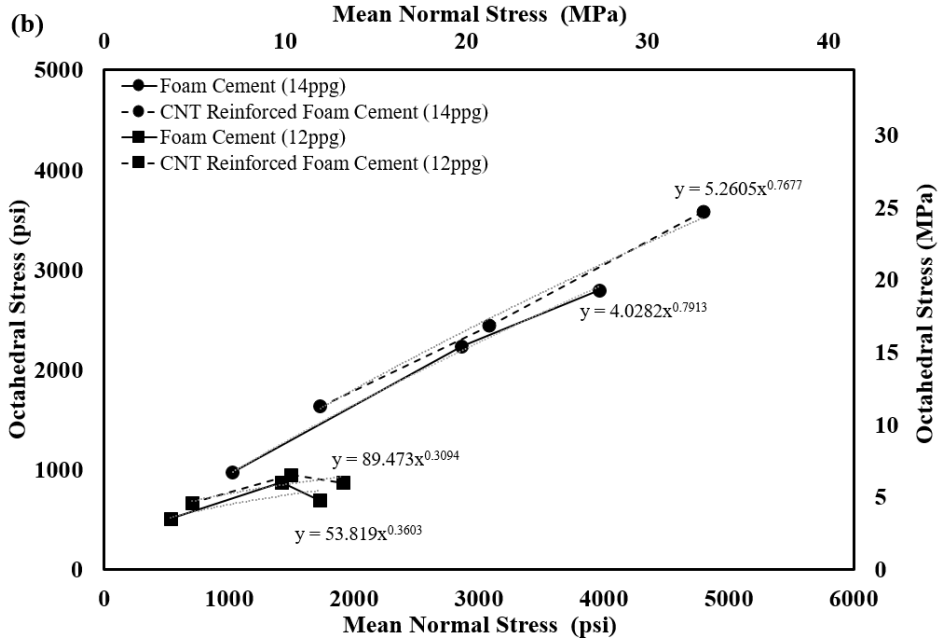

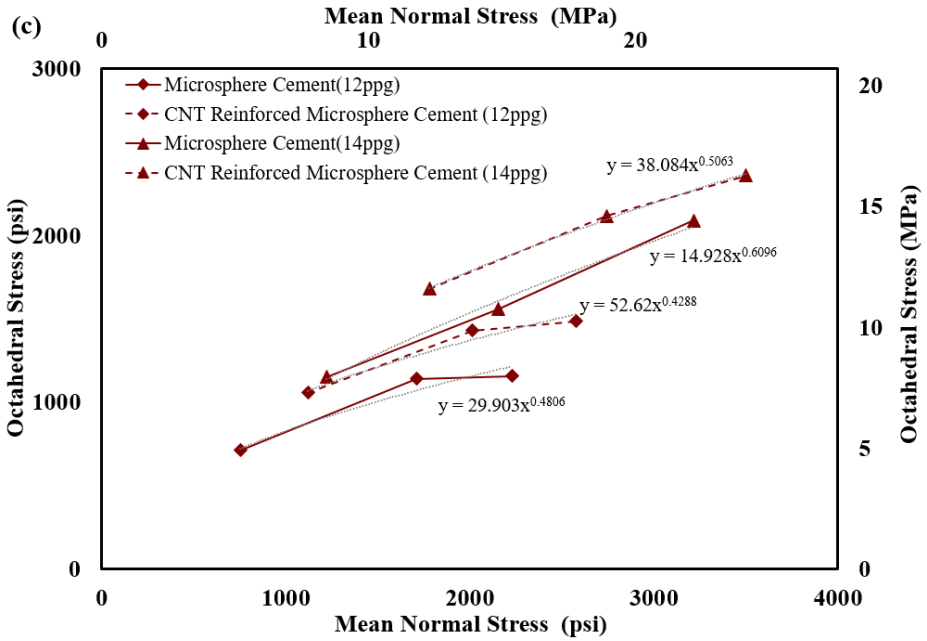

Figure 5.9 The relationship of mean normal stress and octahedral shear pressure of (a) conventional cement systems, (b) foam cement systems, and (c) microsphere cement systems under tri-axial conditions

Table 5.4 The Application of Hamison-Chang Failure Criterion on Different Cement Systems

Cement Sample Type (material)	Density (ppg)	Material Constant A	Material Constant n	R^2	RMSE
Conventional cement	16.2	4.617	0.790	0.9958	386.47
CNT reinforced conventional cement	16.2	7.344	0.741	0.9966	320.57
Foam cement	14	4.028	0.791	0.9992	180.74
CNT reinforced Foam cement	14	5.261	0.768	0.9959	331.52
Foam cement	12	53.819	0.360	0.689	253.45
CNT reinforced Foam cement	12	89.473	0.309	0.7929	155.74
Microsphere Cement	14	14.928	0.610	0.9921	143.99
CNT reinforced foam cement	14	38.084	0.506	0.9979	49.83
Microsphere Cement	12	29.903	0.481	0.9564	163.40
CNT reinforced foam cement	12	52.620	0.429	0.9654	122.54
Water extended conventional cement	14	44.319	0.440	0.9164	199.76

Comparing R-squared values and RMSE of four failure criterion mentioned above, i.e, Drucker-Prager, Mogi-Coulomb, Hoek-Brown, Haimson-Chang failure criterion, we can reasonably arrive at the conclusion that Drucker-Prager and Mogi-Coulomb failure criterion are more suitable to characterize different cement failure mechanism due to their high R-squared value and low RMSE. The relationship of cement ultimate compressive strength and confining pressure can be regarded as linear. Hoek-Brown failure criterion is not a good candidate for cement failure characterization, because of the high RSME, which indicates a big difference between measured compressive strength and model prediction. Haimson-Chang failure criterion is good for failure simulations of conventional and microsphere cement systems, but not for foam cement failure simulations.

5.1.5 Brittleness Index

Brittleness index of oil well cement composite represents the ability to maintain cement integrity under downhole conditions, which reflects the effectiveness of zonal isolation. The brittleness of a cement composite is quantified using the brittleness index defined in Eq. (4.6). A low brittleness index indicates a more ductile cement composite, which is capable to store larger deformations and withstand higher stress perturbations under the same loading condition.

Figure 5.10 shows the brittleness index for different cement systems under elevated confining pressures. From this figure, the brittleness index is highest under uniaxial loading conditions and decreases rapidly with increasing confining pressures. The rate of reduction in brittleness decreases with the introduction of confining pressures. For instance, the brittleness index of foam cement decreases from 0.94 under uniaxial loading to 0.51 under 500 psi confining pressure (46% reduction), and continues to decrease to 0.31 under 1000 psi confining pressure

(39% reduction). Conventional cement shows the lowest brittleness index under uniaxial loading condition compared to other CNT-free cement systems. This trend, however, is reserved when confining pressures are introduced. The addition of CNTs into different cement systems lower the brittleness index, which indicates a higher ductility.

The number of micro cracks and pores in conventional cement is fewer than that of foam and microsphere cement composites, due to its homogenous and continuous phase (Chapter 5.2.1), resulting in fewer stress concentration spots. When an axial load is applied at the two ends of foam and microsphere cement specimens, stress is likely to be concentrated at the locations of air bubbles, microspheres, and micro cracks, resulting in a localized stress increase. Cracks in cement composite are generally started from these stress-concentrated locations. Under uniaxial loading condition (without confining pressure), such cracks, caused by stress concentrations, are easily extended and interconnected, which eventually results in the cement failure. While for the cement specimens tested under confining pressures, micro cracks and pores were hold together and their separation and extension were inhibited under confinement, resulting in lower brittleness index and higher compressive strength.

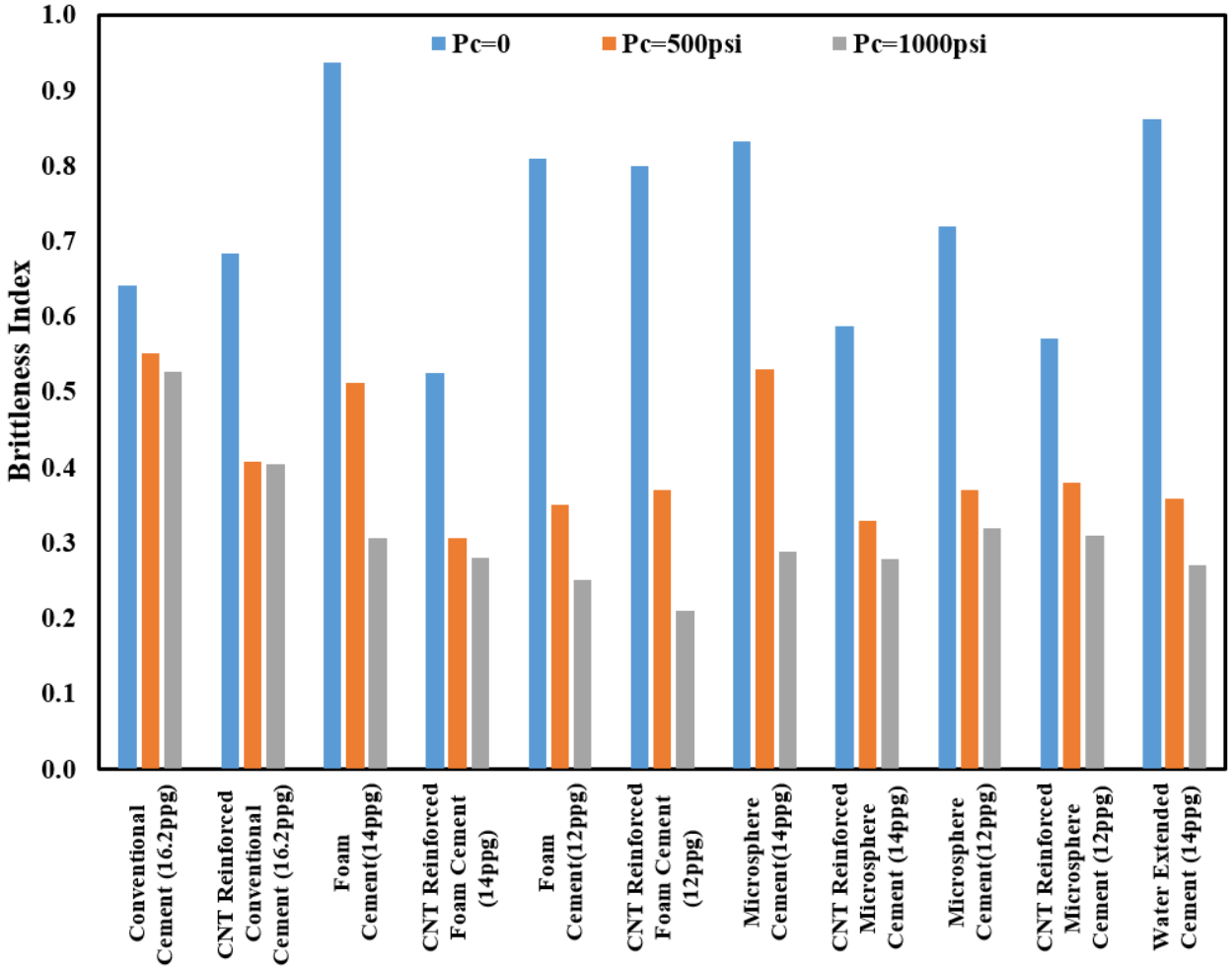

Figure 5.10 Brittleness index of various cement systems under tri-axial conditions

5.1.6 Ultimate Strain Capacity

Figure 5.11 shows the strain capacity of studied cement systems under confining pressures. Strain capacity is defined as the total strain measured at failure point. A high strain capacity represents the ability for cement composite to store a large deformation at failure. From Figure 5.11, the strain capacity of all cement systems increases with confining pressure.

The compressibility of cement samples, as given for comparison of Young's modulus of lightweight and conventional cements, can also be used to explain why the strain capacity of lightweight cement is higher than that of conventional cement. The air-solid structure of

lightweight cements is capable to tolerate larger deformations at failure than the single solid structure of conventional cement. In addition, the CNT-reinforced cements exhibit over 10% improvement in strain capacity compared to their CNT-free compartments, because of the CNTs' bridging mechanism.

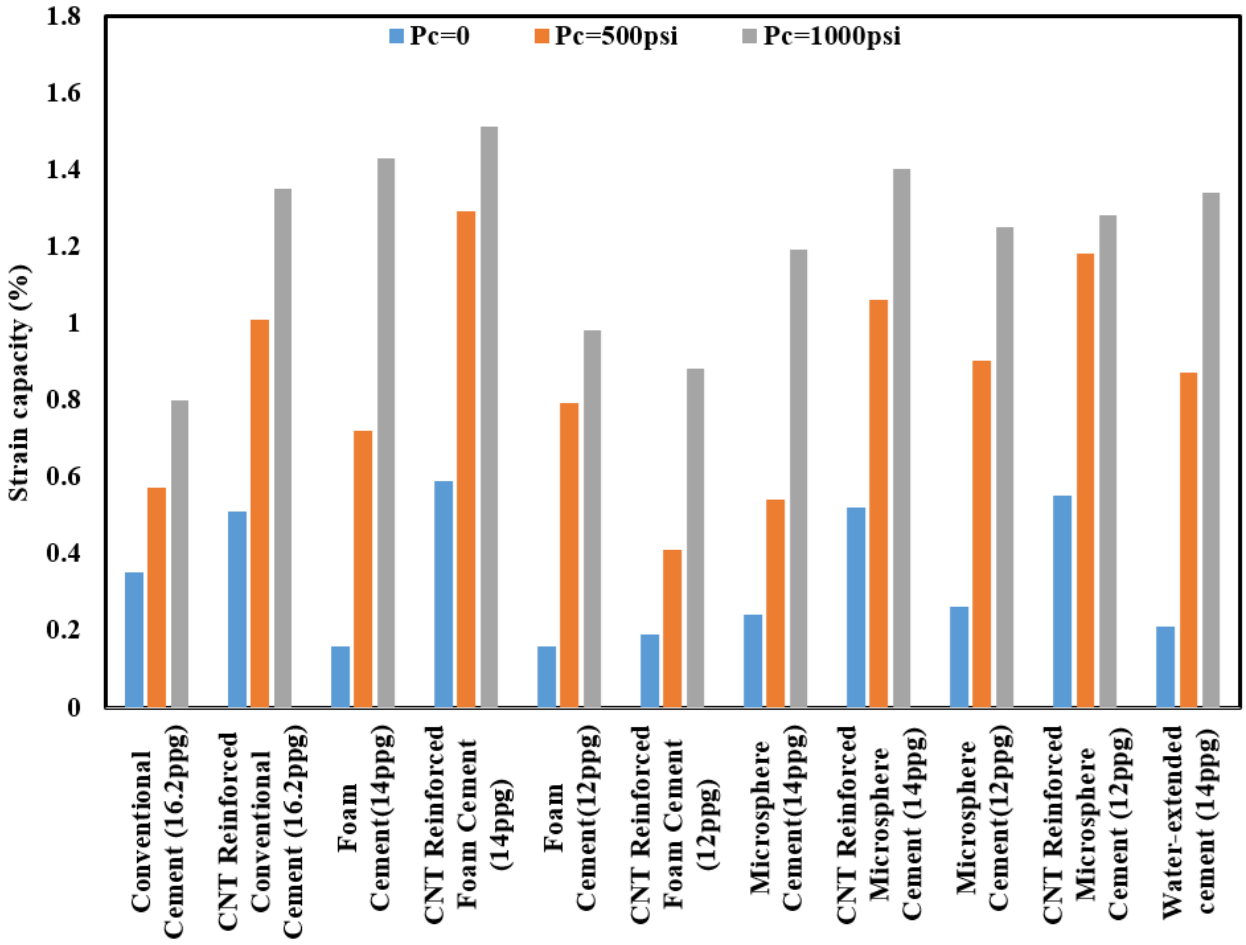

Figure 5.11 Ultimate strain capacity of various cement systems under tri-axial conditions

Besides the addition of CNTs and confining pressure, another factor that affects cement strain capacity is its density. At the density of 14 ppg, foam cement exhibits higher strain capacity than that of microsphere cement. The reason is air bubbles in cement composite have higher compressibility than microspheres. That is, air bubbles are able to store more deformation than microspheres under the same axial and confining pressure conditions. However, when the density

decreases to 12 ppg, microsphere cement outperforms foam cement in terms of strain capacity. Result shows that the strain capacity of foam cement decreases more rapidly than microsphere cement with density. It should be noted that strain capacity is strongly dependent on cement compressive strength. If a cement sample is able to withstand high compressive strength, the value of its strain capacity will increase correspondingly. Compared to the 12 ppg foam cement composite, 12 ppg microsphere cement exhibit higher compressive strength that correlates a higher strain capacity.

5.1.7 Splitting Tensile Strength

Cement sheath may undergo different loading conditions due to seismic activities, remedial cementing, etc. Therefore, splitting tensile strength tests provides another strength properties to evaluate cement integrity. The tensile strength of cement specimens was evaluated using the splitting tensile testing facility under ambient condition.

Results of splitting tensile strength of all cement systems are shown in Figure 5.12. Generally, the tensile strength of cement composite is over ten times lower than compressive strength due to its brittle nature. Adding extra water into conventional cement to extend its density from 16.2 ppg to 14 ppg gives little satisfaction in strength properties. The conventional cement bears higher splitting tensile strength than any lightweight cement systems, because of its compact solid structure. Light-weighting conventional cements by adding air bubbles and microspheres decreases cement splitting tensile strength. Results also show that the splitting tensile strength of all cements increases from 5 to 33% with the addition of CNTs.

On average, the splitting tensile strength of all 14 ppg foam and microsphere cement specimens is about 189 psi with a standard deviation of 11 psi. The splitting tensile strength of all

12 ppg foam and microsphere cement specimens is about 123 psi with a standard deviation of 3 psi.

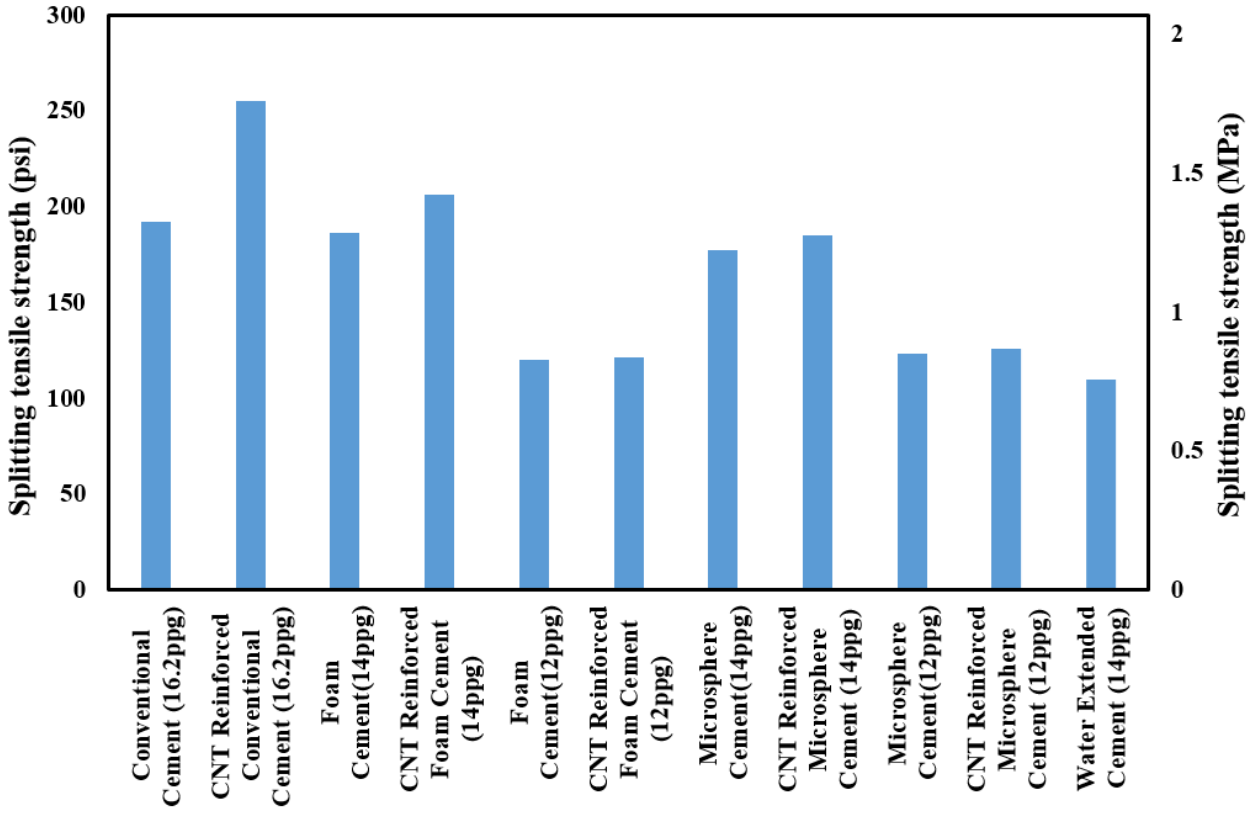

Figure 5.12 Splitting tensile strength of various cement systems

5.1.8 Permeability

To measure the conductivity of cement to the flow of fluid, the permeability of cement specimens were evaluated using tri-axial rock mechanics facility. Figure 5.13 shows the plots of flow rate vs. time and pressure vs. time for CNT-reinforced foam cement, respectively. The solid and dashed graphs in Figure 5.13(a) represent the inflow and outflow flow rates from two pore pressure intensifiers. A pressure difference was imposed on top and bottom of the cement specimens. Once the flow rate and pressure difference are stabilized, the permeability is evaluated. An example of CNT reinforces foam cement is shown in Figure 5.13(a), the stabilized volumetric

flow rate through cement specimen is 0.0025 cc/min under a constant pressure difference of 72 psi during the time from 30 to 35 min. According to Darcy's law in Eq. (4.3), the permeability is calculated to be 0.25 md. Table 5.5 summarizes permeability of the rest studied cement specimens.

As shown in Table 5.5, conventional cement and water extended cement are impermeable due to their continuous solid phases. The permeability of foam and CNT-reinforced foam cement with the density of 14 ppg are 0.52 md and 0.25 md, respectively. As the density of foam cement goes lower, a higher permeability was observed. Foam cement is a permeable medium, because of the dispersed air bubbles in solid phase. Air bubbles may interconnect to each other and provide a tortuous channel for fluid flow through. A reduction in permeability of foam cement with the addition of CNTs was observed. CNTs entangle together and function as plugging nanofibers in foam cement composite and results in a reduced permeability. Though microsphere cement composite has air-solid structure, the fluid movements are inhibited by the impermeable glass walls of hollow glass microspheres, resulting in an impermeable medium.

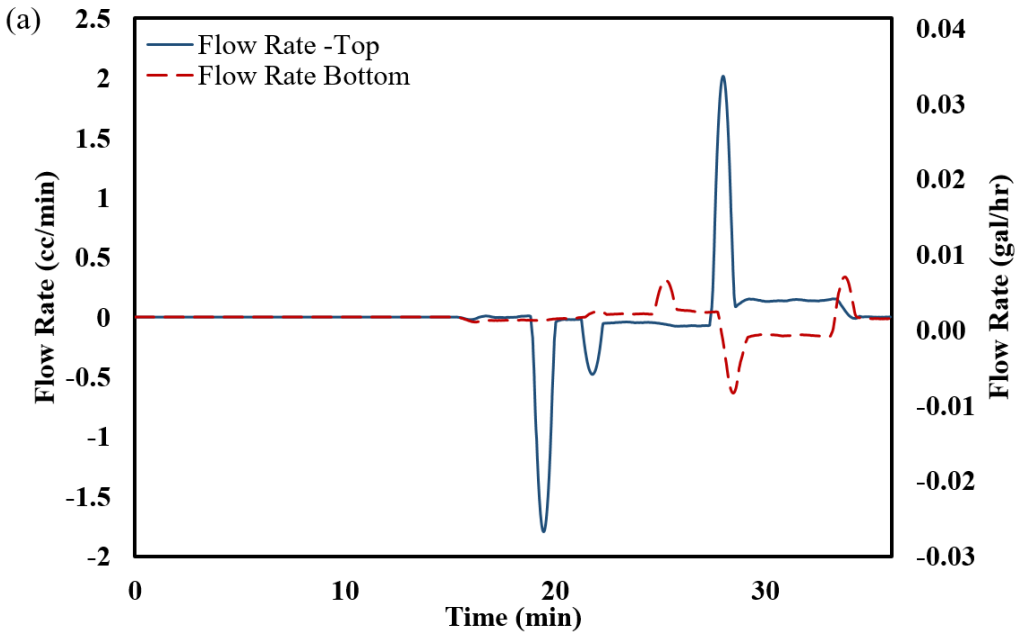

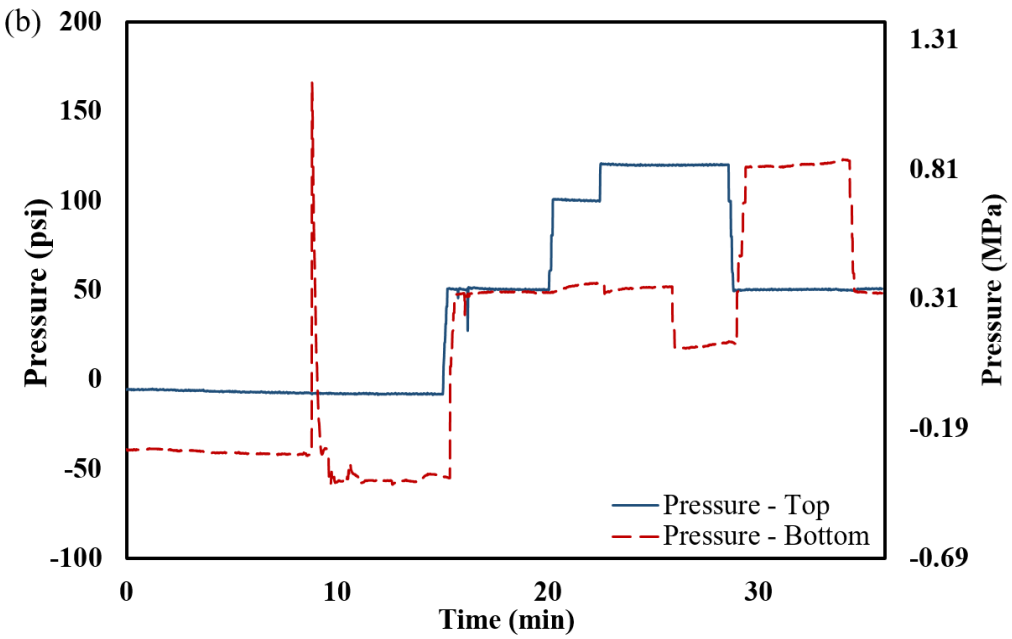

Figure 5.13 Measured flow rates and pressures of CNT-reinforced cement specimens for the calculation of permeability

Table 5.5 Permeability of cement specimens

Cement Sample Type (material)	Density (ppg)	Permeability (mD)
Conventional cement	16.2	0
CNT reinforced conventional cement	16.2	0
Foam cement	14	0.52
CNT reinforced foam cement	14	0.25
Foam cement	12	0.76
CNT reinforced foam cement	12	0.58
Microsphere cement	14	0
CNT reinforced microsphere cement	14	0
Microsphere cement	12	0
CNT reinforced microsphere cement	12	0
Water extended conventional cement	14	0

5.1.9 Porosity

Porosity is an evaluation of the compactness of cement sheath. A lower porosity indicates a more compact cement material, which is more effective in providing zonal isolation by preventing gas, water and hydrocarbon migrations. Gas, water and other hydrocarbons reside into cement natural pores, intrinsic cracks and gaps during oil production, which changes the stress condition in cement sheath.

A typical pores distribution for hardened cement sample contains pores and cracks with different sizes, shapes and interconnectivities. As shown in Figure 5.14, the pore spaces in cement composite is comprised of air bubbles that are blended into cement slurry during mixing, gel pores that are generated during slurry hydration, and interconnected capillary pores that result in permeability [52]. Capillary pores, ranging from 10 nm to 50 nm, are void spaces between cement grains that provide tortuous channels for gas and fluid to flow through. Gel pores, ranging from 0.5 nm to 10 nm, formed by water evaporation during cement hydration that constitute the internal porosity of the gel phase.

As shown in Table 5.6, the addition of microspheres and CNTs has negligible effect on cement porosity. Water extended cement sample shows a relatively high porosity. The reason behind this phenomenon could be the increased volume of gel pores in cement composite with a high water ratio. Foam cement samples have much higher porosity than non-foamed ones, because of the well dispersed air bubbles that are over 100 times bigger than capillary and gel pores. Each air bubble in hardened foam cement composite can be regarded as a small reservoir.

It is necessary to note the limitations of cement porosity measurement. Water cannot infiltrate into every single void space in cement composite. Some pore spaces are located too far from the outer surface and are isolated in the pore network. The tortuous narrow channels pose

frictional force to restrict water from infiltrating in. Porosity tests were conducted under ambient conditions. Some of the initial air bubbles in micro cracks inside cement composite are attached to the cement walls and are hard to move out. It is believed that the measured porosity is lower that the true value of cement total porosity.

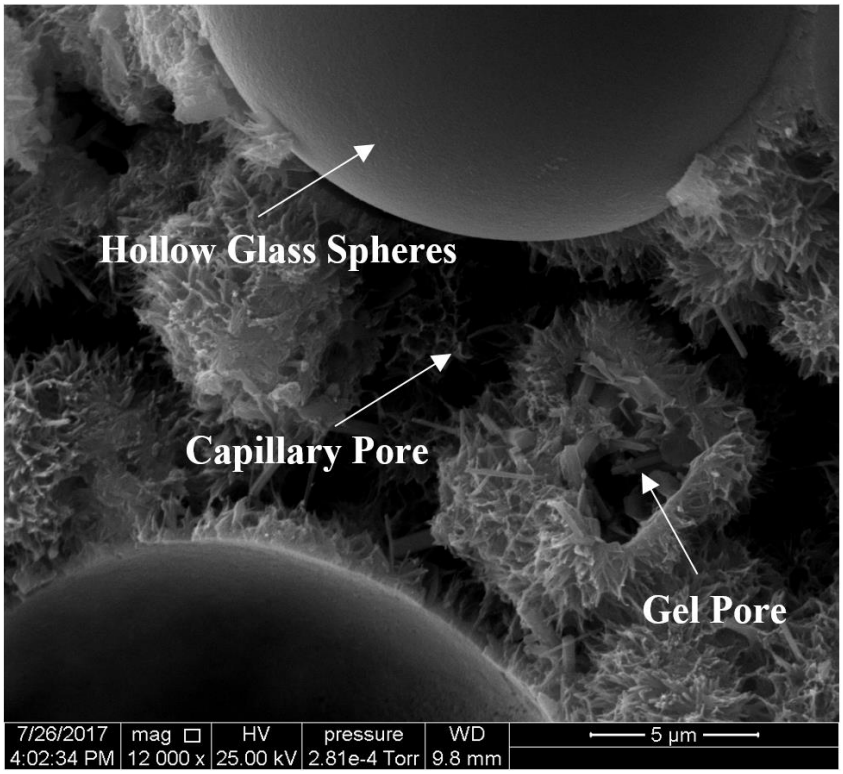

Figure 5.14 Pore Spaces in Cement Composites

Table 5.6 Porosity of cement specimens

Cement Sample Type (material)	Density (ppg)	Measured Porosity (%)
Conventional cement	16.2	12.3
CNT reinforced conventional cement	16.2	12.0
Foam cement	14	16.0
CNT reinforced foam cement	14	16.4
Foam cement	12	21.6
CNT reinforced foam cement	12	20.8
Microsphere cement	14	10.6
CNT reinforced microsphere cement	14	11.2
Microsphere cement	12	11.8
CNT reinforced microsphere cement	12	10.4
Water extended conventional cement	14	14.7

5.2 Cement Microstructure Observations

5.2.1 Structural Difference among Cement Systems

Figure 5.15 shows the Scanning Electron Microscope (SEM) images of micro structures of (a) 16.2 ppg conventional cement, and (b) 14 ppg water extended cement at the magnification scale of 400X. Both SEM images show continuous solid phase without any air bubbles or micro cracks, resulting in impermeable cement mediums. SEM images of microsphere cement at 14 ppg and 12 ppg are shown in Figure 5.16. A higher concentration of hollow glass spheres was observed in the SEM image of 12 ppg microsphere cement. Hollow glass spheres (type 8000X) are ultra-strong glass bubbles with a crush resistance of 8000psi. However, few broken hollow glass spheres was found in Figure 5.17, possibly resulting from cement mixing or tri-axial compressive strength testing. Figure 5.18 shows the SEM images of micro structures of foam cement with the densities of 14 ppg and 12 ppg. Fewer air bubbles with smaller sizes were observed in 14 ppg foam cement, compared to 12 ppg foam cement. Air bubbles have tendency to aggregate, merge and collapse during setting period of foam cement slurry, which result in higher permeability, lower strength properties and higher density. Signs of bubbles coalescence were observed (Figure 5.18).

Foam and microsphere cements exhibit different microstructures due to different light-weighting techniques. Microsphere cement shows uniformly dispersed small glass bubbles in cement composite, while air bubbles dispersed in foam cement specimens shows variable bubble shapes and sizes with signs of coalescence.

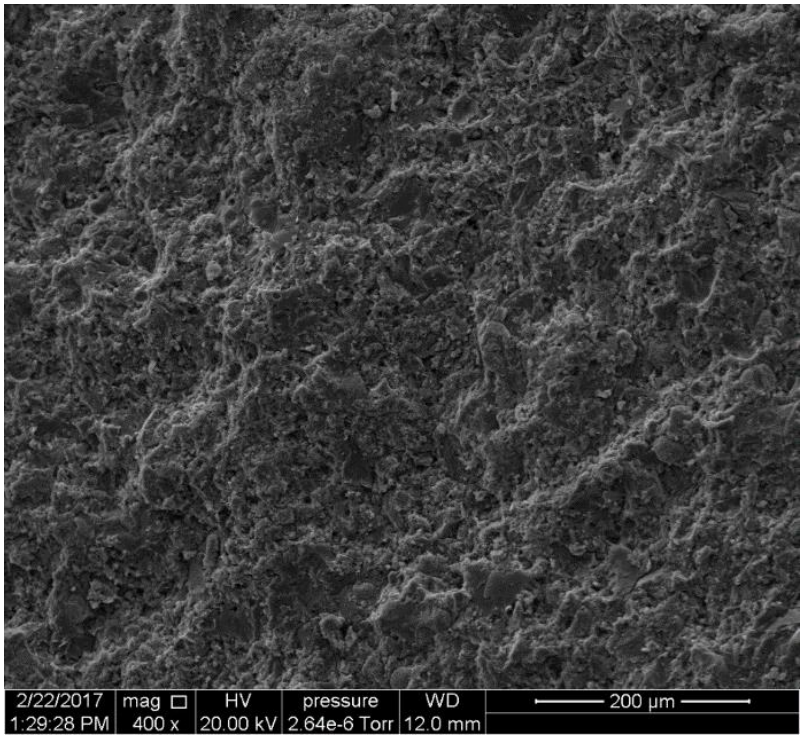

(a)

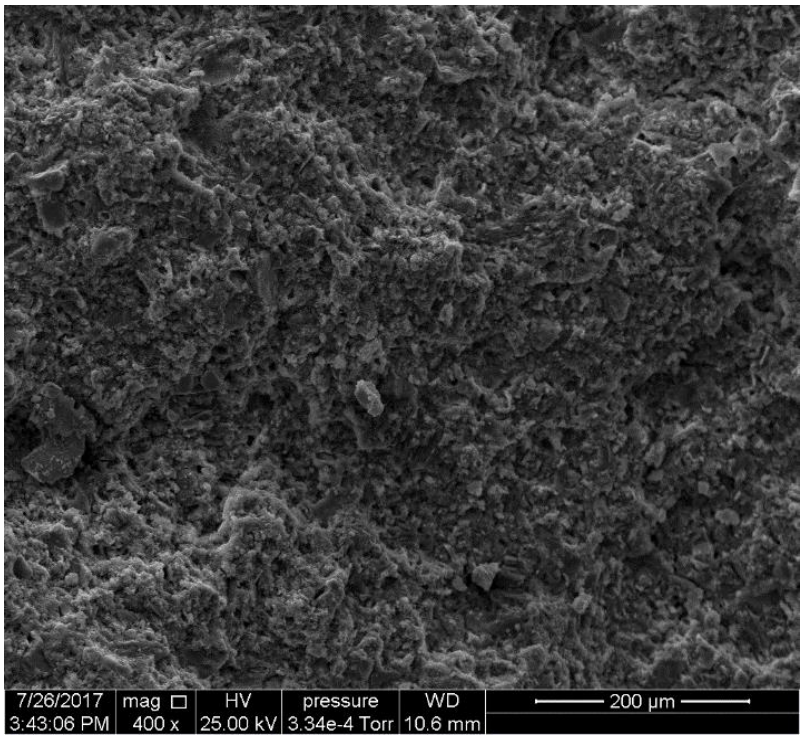

(b)

Figure 5.15 SEM images of (a) conventional cement (16.2 ppg) and (b) water extended conventional cement (14 ppg)

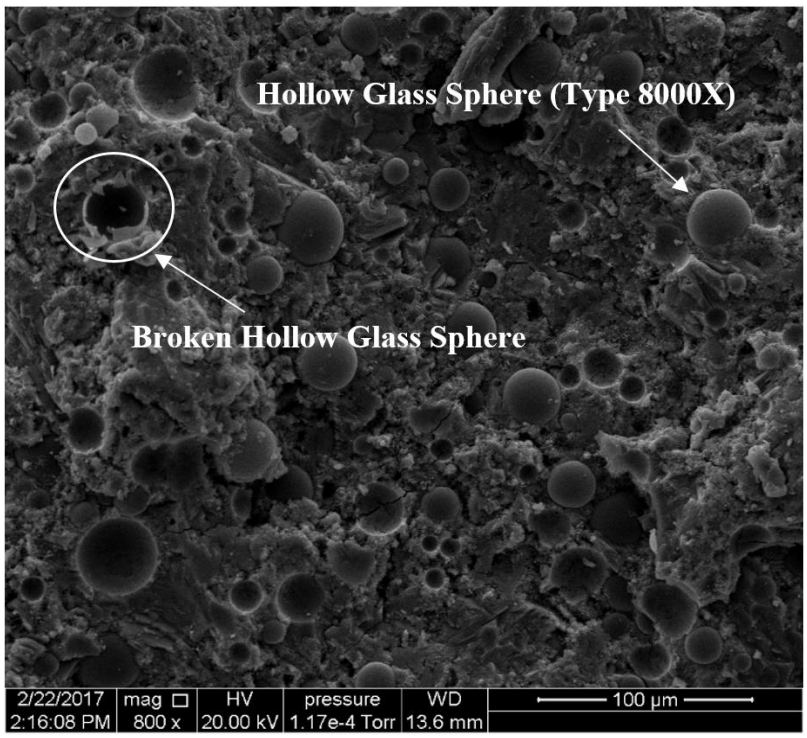

(a)

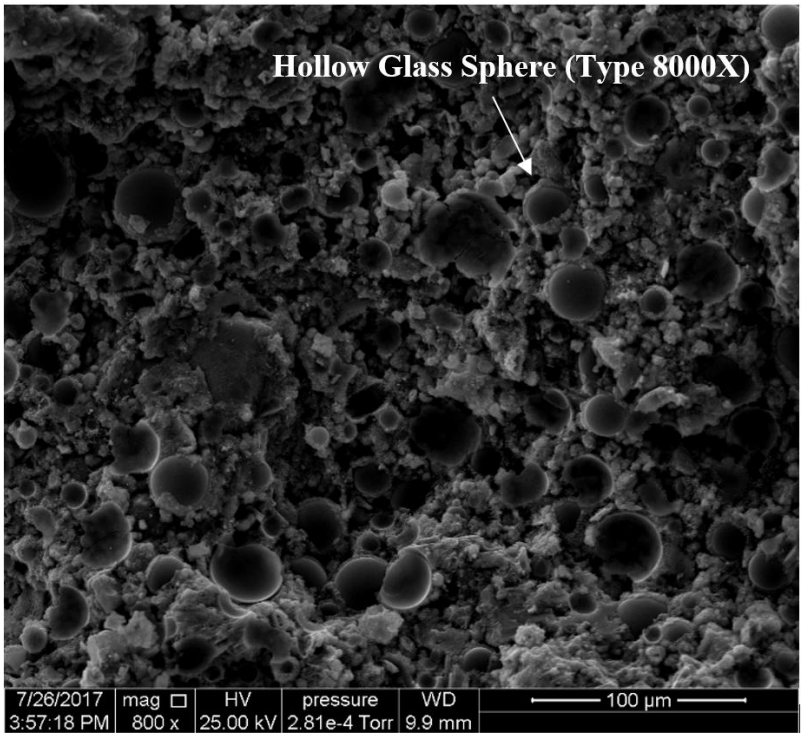

(b)

Figure 5.16 SEM images of microsphere cements with the densities of (a) 14 ppg and (b) 12 ppg

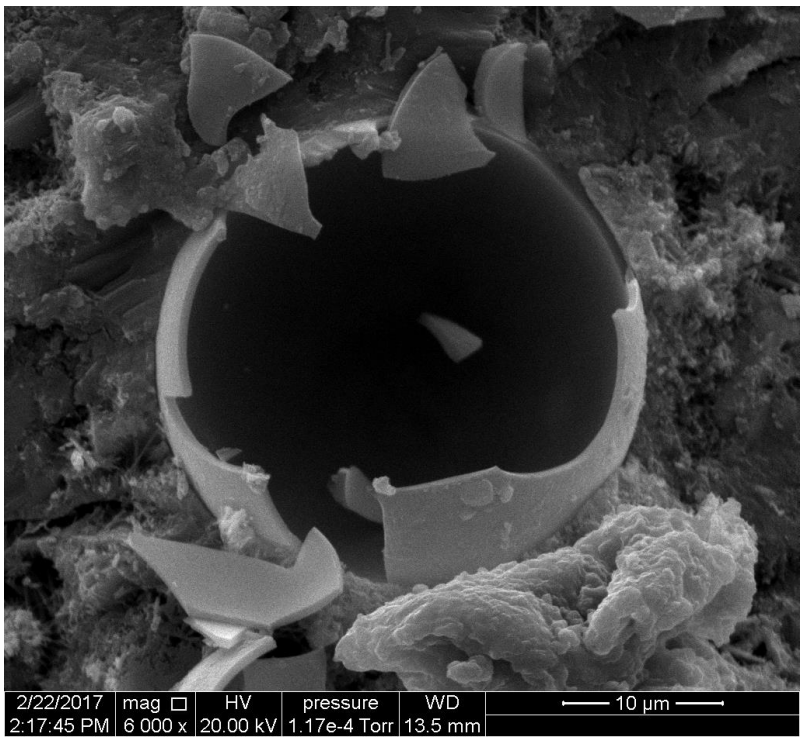

Figure 5.17 Broken hollo glass sphere

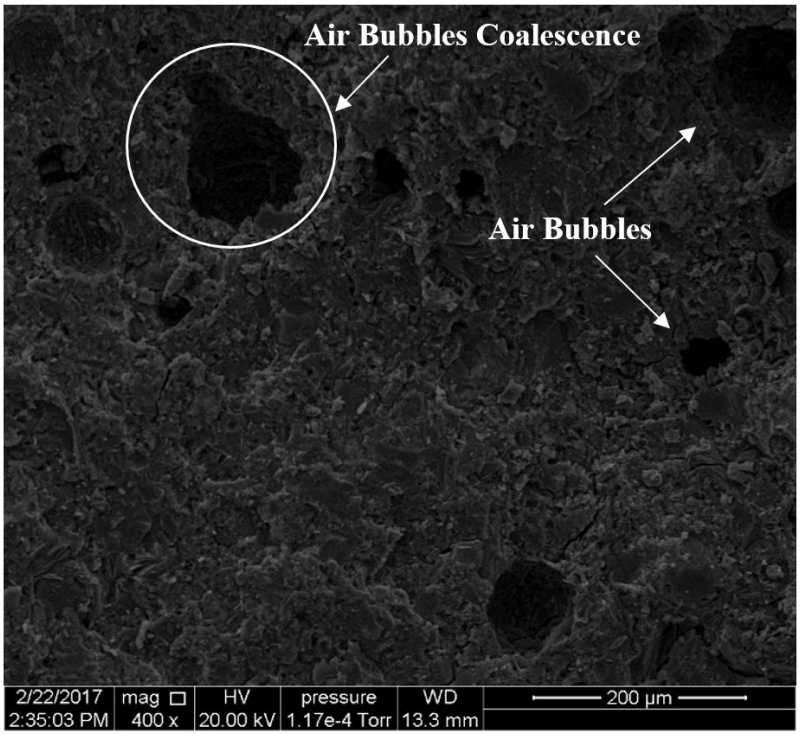

(a)

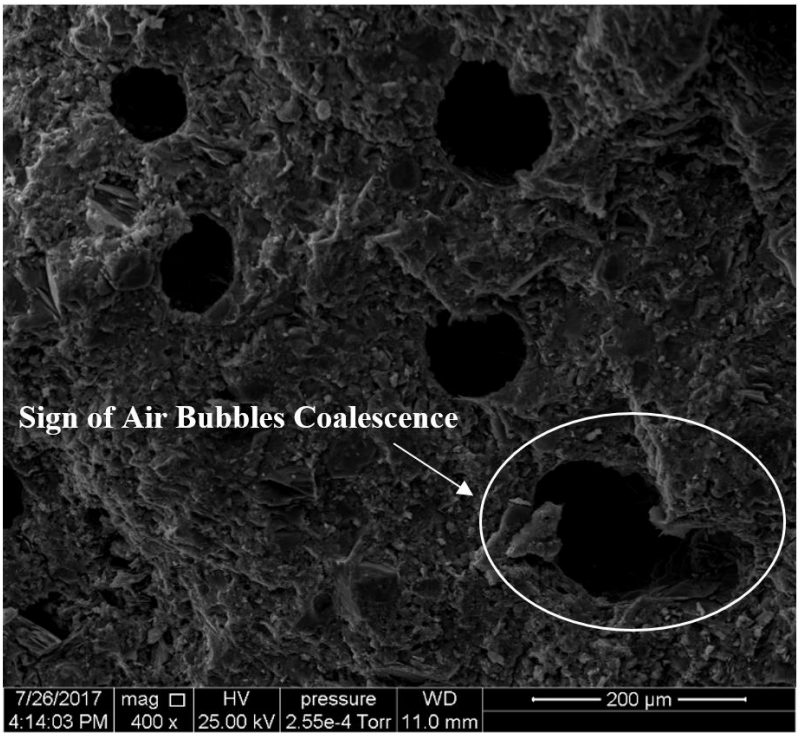

(b)

Figure 5.18 SEM images of foam cements with the densities of (a) 14 ppg and (b) 12 ppg

5.2 CNTs' Bridging and Plugging Effects

The SEM image of conventional cement reinforced by 0.5%bwoc CNT is shown in Figure 5.19. A micro crack bridged by CNT along with its approximate diameter has been shown in this figure. Micro cracks are generated during two different stages: 1) cement setting period by chemical reactions and initial stress development, and 2) compressive strength testing process by applied axial load. When a micro crack is generated in cement specimens, CNT functions as a bridge connecting two walls of the crack and inhibits one wall from being pulled further from another wall until one end of CNT is detached. A macro crack, which result in cement failure, is formed by accumulation of micro cracks. The overall strength and strain capacity are improved by well-dispersed CNTs through bridging micro cracks in cement sheath.

A micro crack and CNT-filled pores are shown in Figure 5.20. Few CNTs were found in the micro cracks, while high concentrations of CNTs were observed in micro pores. Due to the high aspect ratio and strong van der Waals interaction energy as high as 0.285eV/A [53], CNTs tend to entangle and bundle together during cement slurry mixing and setting period. Such entanglement prevents cement slurry from infiltrating in, which results in void spaces (pores) filled with CNTs in cement composite. However, no cracks starting from CNT-filled pores were observed under SEM, which possibly proves these micro pores formed by CNTs entanglement are strengthened by the filled CNTs. The majority of cracks observed were shown in areas with low concentration of CNTs (Figure 5.21). CNTs function as bridges connecting and plugging the micro cracks and pores, resulting in higher strength and lower permeability, which are in accordance with the permeability and compressive strength data shown in Chapter 5.1.

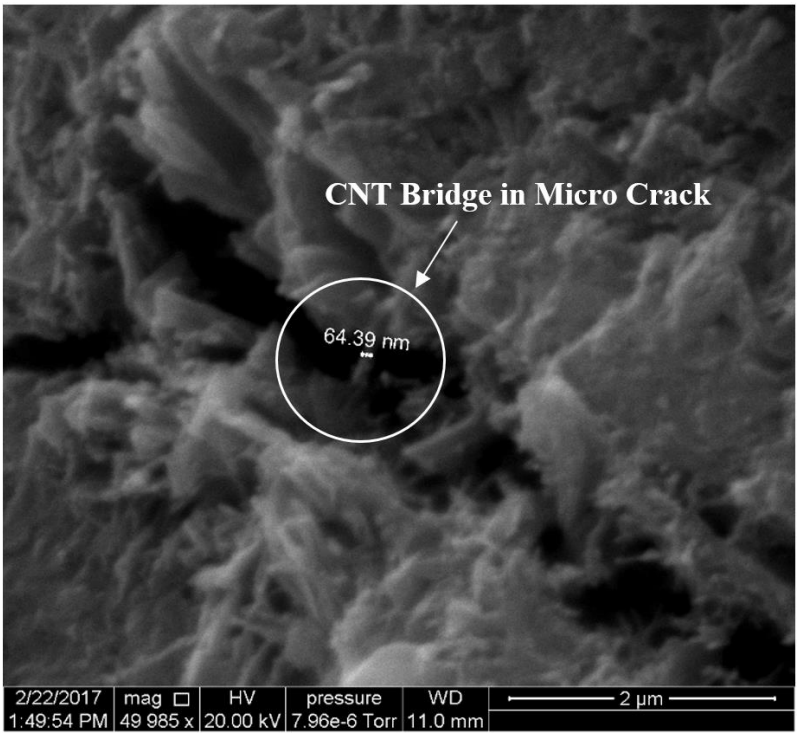

Figure 5.19 SEM image of CNT bridged micro crack and CNT size measurement

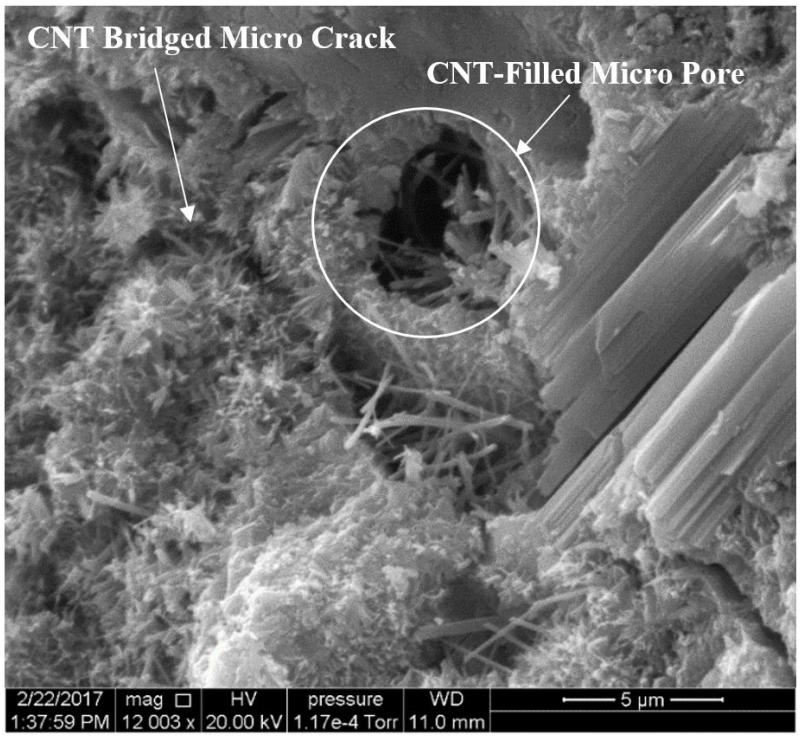

Figure 5.20 SEM image of CNT-filled micro crack and pores

Figure 5.21 SEM image of a micro crack in low CNT concentrated area

5.3 Rheological Properties

RS300 rheometer was designed for the rheology measurement under flow through and pressurized conditions. In this study, RS300 was used for the rheology measurement of conventional cement, CNT reinforced conventional cement and water extended cement slurries. To avoid excessive free water in water extended cement slurry, 1 %bwoc bentonite was added to counteract the increased water ratio.

RS300 stopped working after the rheology tests of conventional cement systems. To continue the rheology study, an alternative rheometer, OFITE M900, was used for the rest rheology measurements of foam and microsphere cement slurries. However, unlike RS300 rheometer, OFITE M900 viscometer only measured the cement rheology under ambient conditions. Foam coalescence could not be compensated during rheology tests, resulting in a lower shear stress and viscosity measurement.

The data and plot of shear rate vs shear stress of conventional, foam and microsphere cement systems are shown in Table 5.7, Table 5.8, Table 5.9 and Figure 5.22. Herschel-Bulkley model was used for rheology characterizations were based on, whose related parameters are shown in Table 5.10. Herschel-Bulkley model is expressed as:

$$\tau = \tau_o + K\,\gamma^n \qquad (5.24)$$

Viscosity is defined as shear rate over shear stress. As can be seen in Figure 5.23, the addition of CNTs into cement slurries increases the viscosity. However, the viscosity increment is not significant and can be counteracted by increased centration of dispersant. The viscosity of foam cement increases with foam quality. That is, low-density foam cement slurry has relatively higher viscosity than high-density foam and its base cement slurries. The addition of microspheres into base cement slurry increases the apparent viscosity, because of the high surface area of hollow

glass spheres. In this project, 12 ppg microsphere cement required a higher water ratio than 14ppg microsphere cement and its base cement slurries. Observation shows that 12ppg microsphere cement slurry exhibits lower viscosity than 14 ppg one, possibly resulting from increased water ratio, which was more effective on increasing microsphere cement rheology than the concentration of microspheres.

Table 5.7 Rheology data of conventional cement systems

			Conventional Cement Slurry	CNT-Reinforced Conventional Cement Slurry	Water-extended Conventional Cement Slurry
Density (ppg)			16.2	16.2	14
Water Ratio (%bwoc)			38	38	55
Bentonite(%bwoc)			-	-	1
Viscometer (RS300)	Speed (rpm)	Shear Rate (1/s)	Shear Stress (Pa)		
	3	3.31	5.85	13.35	4.51
	6	6.62	8.17	13.97	4.90
	30	33.08	9.58	20.38	7.00
	60	66.16	15.99	24.81	8.64
	100	110.3	18.99	28.09	11.43
	200	220.5	25.99	33.40	16.08
	300	330.8	34.31	39.20	21.06

Table 5.8 Rheology data of foam cement systems

			Foam Cement Slurry		CNT-Reinforced Foam Cement Slurry	
Density (ppg)			14	12	14	12
Water Ratio (%bwoc)			38	38	38	38
Foaming Agent (%bwoc)			0.26	0.32	0.26	0.32
Viscometer (OFITE)	Speed (rpm)	Shear Rate (1/s)	Shear Stress (Pa)			
	3	5.11	6	7.5	6.3	8.2
	6	10.21	8.2	9.8	9.7	11.4
	30	51.07	12.3	17.1	15.1	18.9
	60	102.14	18.1	25.6	19.9	27.2
	100	170.23	24.6	33.1	26.9	35.1
	200	340.46	35.3	47.5	37.8	53.5
	300	510.69	46.1	59.2	50.8	65.5

Table 5.9 Rheology data of Microsphere cement systems

			Microsphere Cement Slurry		CNT-Reinforced Microsphere Cement Slurry	
Density (ppg)			14	12	14	12
Water Ratio (%bwoc)			38	46	38	46
HGS 8000X (%bwoc)			4.56	11.95	4.56	11.95
Viscometer (OFITE)	Speed (rpm)	Shear Rate (1/s)	Shear Stress (Pa)			
	3	5.11	10.7	12.0	7.5	9.9
	6	10.21	12.9	15.5	9.4	11.4
	30	51.07	22.8	27.5	15.6	19.0
	60	102.14	34.8	41.3	24.3	28.3
	100	170.23	48.3	51.8	31.9	39.7
	200	340.46	71.6	82.8	50.2	59.8
	300	510.69	89.8	107.2	64.1	71.4

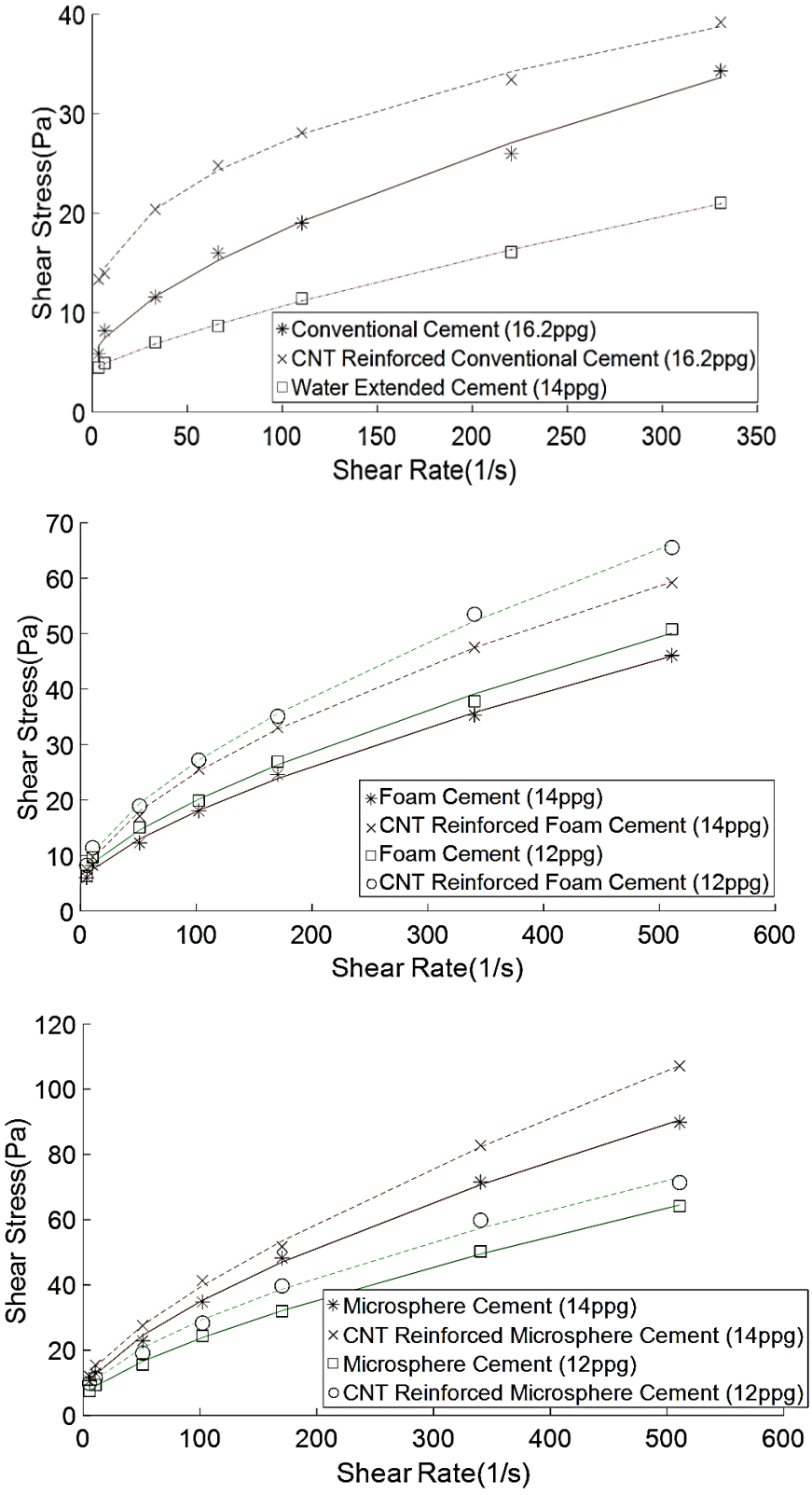

Figure 5.22 Rheology of (a) conventional cement systems, (b) foam cement systems, and (c) microsphere cement systems

Table 5.10 Rheology Characterizations of various cement systems

Cement Sample Type (material)	Density (ppg)	Herschel-Bulkley Model Parameters			
		Consistency Factor K	Flow Behavior Index n	Yield Stress τ_o	Relations
Conventional cement	16.2	0.664	0.648	5.21	$\tau = 5.21 + 0.66\,\gamma^{0.65}$
CNT reinforced conventional cement	16.2	3.171	0.392	7.897	$\tau = 7.9 + 3.17\,\gamma^{0..39}$
Foam cement	14	0.526	0.699	4.771	$\tau = 4.77 + 0.53\,\gamma^{0.7}$
CNT reinforced Foam cement	14	1.214	0.612	4.368	$\tau = 4.37 + 1.21\,\gamma^{0.61}$
Foam cement	12	0.618	0.688	5.501	$\tau = 5.5 + 0.62\,\gamma^{0.7}$
CNT reinforced Foam cement	12	1.142	0.637	5.454	$\tau = 5.45 + 1.14\,\gamma^{0.64}$
Microsphere Cement	14	1.375	0.660	6.132	$\tau = 6.13 + 1.38\,\gamma^{0.66}$
CNT reinforced foam cement	14	1.254	0.700	8.484	$\tau = 8.48 + 1.25\,\gamma^{0.7}$
Microsphere Cement	12	0.652	0.723	5.401	$\tau = 5.4 + 0.65\,\gamma^{0.72}$
CNT reinforced foam cement	12	1.113	0.655	6.023	$\tau = 6.02 + 1.11\,\gamma^{0.66}$
Water extended conventional cement	14	0.17	0.792	4.135	$\tau = 4.77 + 0.53\,\gamma^{0.7}$

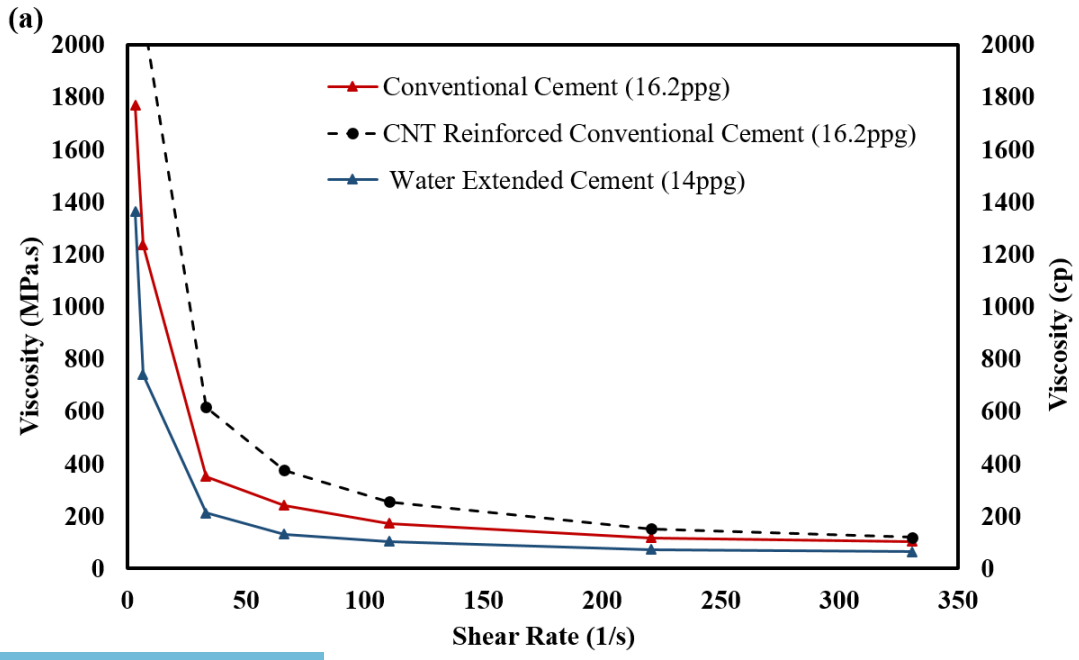

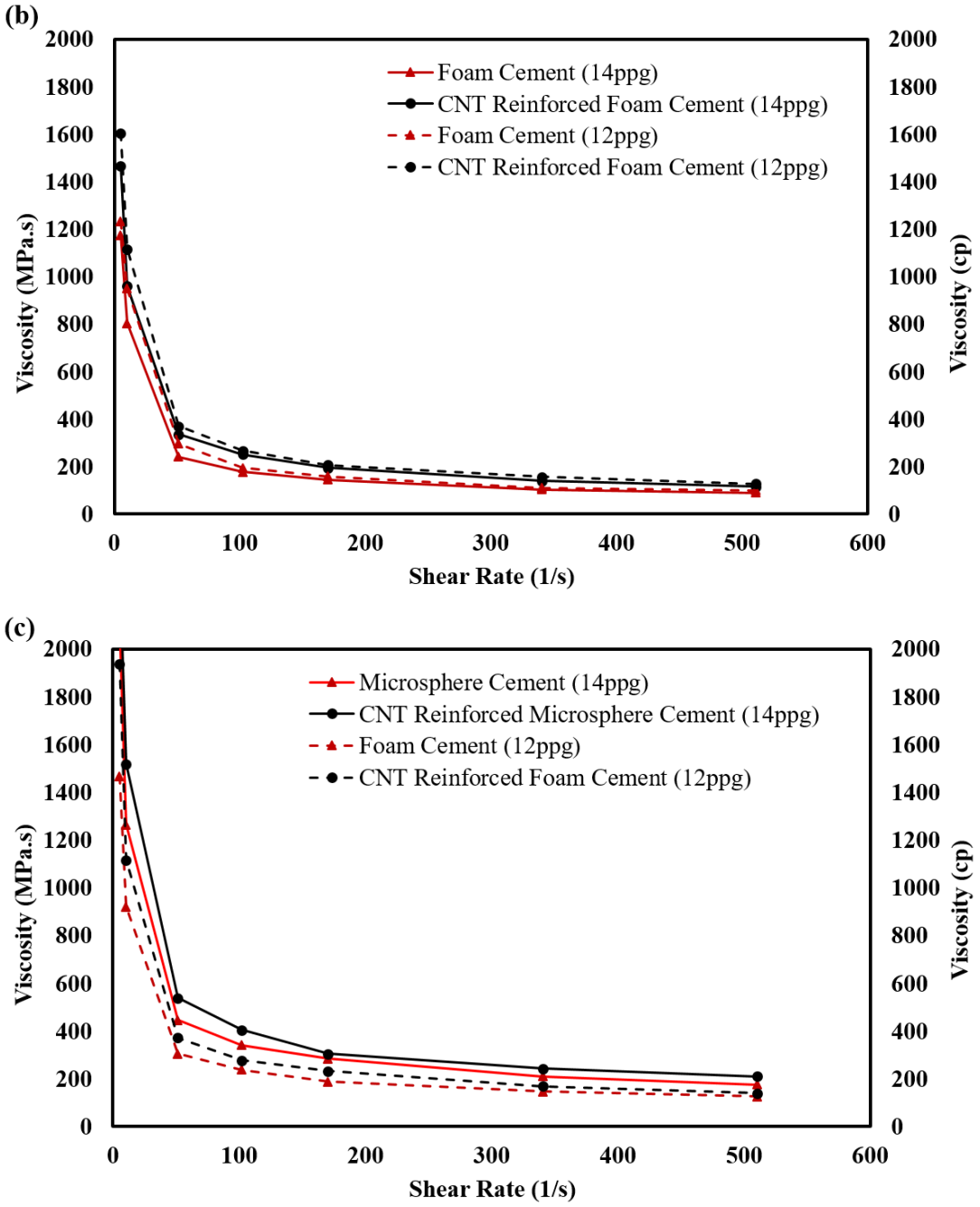

Figure 5.23 Viscosity of (a) conventional cement systems, (b) foam cement systems, and (c) microsphere cement systems

5.4 Cement Stability

5.4.1 Stability of Unset Slurries

A well-sealed standard 250-ml graduate cylinder, shown in Figure 5.24, was used for stability test of unset foam cement slurry. No volume change of foam and CNT reinforced foam cement slurries with the densities of 12 ppg and 14 ppg was observed after a 2-hour waiting period.

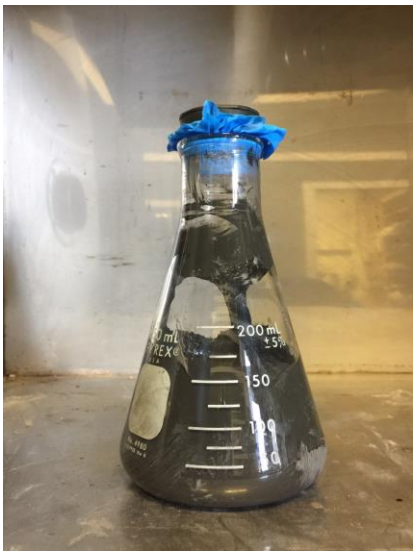

Figure 5.24 Stability test of unset foam cement slurry

8-in PVC tubes with two end seal caps were used as curing mold. Cement slurry was cured under constant 100^{o}F temperature for 72 hours to avoid thermal shock induced stress fractures. As shown in Figure 5.24, foam cement samples with the densities of 12 ppg and 14 ppg exhibit zero volume reduction after curing period, which indicate stable foam cement systems.

Figure 5.25 Hardened foam cement with the densities of 12 ppg (left) and 14 ppg (right)

5.4.2 Stability of Hardened Cement

As recommended by API 10B-4 standard, stability of hardened foam cement was measured by the density of each section along the curing mold (Figure 5.26). Table 5.11 presents the stability measurement if lightweight cements. As shown in Table 5.11, the density variation among each section is less than 3%, which indicate stable lightweight cement systems.

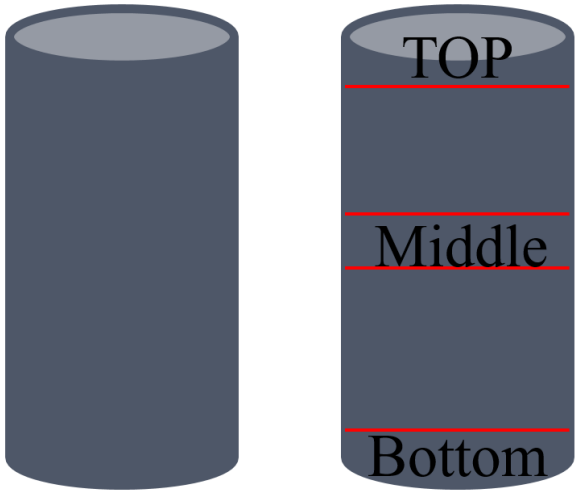

Figure 5.26 Diagram of hardened cement stability measurement

Table 5.11 Stability measurement of lightweight cements

		Section 1 (Top)	Section 2 (Middle)	Section 3 (Bottom)
CNT Reinforced Foam Cement (14 ppg)	Volume (cc)	12.10	11.45	10.10
	Weight (g)	20.85	19.77	17.6
	Density (g/cc)	1.723	1.727	1.743
CNT Reinforced Foam Cement (12 ppg)	Volume (cc)	11.50	13.20	11.85
	Weight (g)	16.36	19.17	17.11
	Density (g/cc)	1.423	1.452	1.444
CNT Reinforced Microsphere Cement (14 ppg)	Volume (cc)	15.10	13.45	17.20
	Weight (g)	25.35	22.60	29.12
	Density (g/cc)	1.679	1.680	1.693
CNT Reinforced Microsphere Cement (12 ppg)	Volume (cc)	10.80	14.70	12.30
	Weight (g)	15.41	20.87	17.65
	Density (g/cc)	1.427	1.420	1.435

CHAPTER 6

CONCLUSIONS AND RECOMMENDATIONS FOR FUTURE WORKS

6.1 Conclusions

The effect of CNTs on the rheology and mechanical properties of lightweight cements were investigated in this study.

Based on the test results, the following conclusions can be drawn:

- Young's modulus of lightweight cements is lower than that of conventional cement, which can be attributed to the ability of lightweight cements to tolerate larger deformation at the same level of axial loading due to their air-solid structure. The addition of CNTs into lightweight cements, however, shows slight effect on Young's modulus.
- Young's modulus is strongly affected by cement density, instead of confining pressure and different lightweight techniques. Foam and microsphere cement systems with the same density exhibit similar values of Young's modulus.
- The compressive strength and strain capacity of hardened cement increase with confining pressure, which means higher strength and stain capacity are attainable at higher well depths.
- Foam, microsphere, and water extended cement systems exhibit higher strain capacity and lower (compressive and splitting tensile) strength, compared to their base phase – conventional cement. Water extended cement gives little compressive and splitting tensile strength satisfaction due to its elevated water ratio.

- The addition of CNTs improves compressive strength, splitting tensile strength and elastic properties of cement composites. Increments in ultimate strain capacity and reductions in brittleness index were observed, resulting from the addition of CNTs. SEM images show the bridging effect of CNTs in cement micro cracks, which makes cement stronger, more elastic and more resistant under stress changes.
- Foam cement outperforms microsphere cement in terms of compressive strength and splitting tensile strength at the same density of 14 ppg. However, when the density is lowered to 12 ppg, microsphere cement exhibit higher strength and elastic properties.
- Drucker-Prager and Mogi-Coulomb failure criterion are more suitable to characterize different cement failure mechanism. The relationship of cement ultimate compressive strength and confining pressure can be regarded as linear. Hoek-Brown failure criterion is not a good candidate for cement failure characterization, because of the high RSME, which indicates a big difference between measured compressive strength and model prediction. Haimson-Chang failure criterion is good for failure simulations of conventional and microsphere cement systems, but not for foam cement failure simulations.
- Only foam cement shows small values of permeability, which is affected by the foam cement density and the addition of CNTs. Conventional and microsphere cements are believe to be impermeable mediums.
- The addition of CNTs and microspheres has negligible effects on cement porosity. Foam cement and water extend cement exhibit higher porosity, because of lager inner void spaces formed by air bubbles and water evaporation, respectively.
- SEM images show that microspheres cements are more homogeneous than foam cements, in terms of bubble size and dispersion.

6.2 Recommendations for Future Works

There are several aspects that still remain unclear and need more research in the future.

- Cement Material Components

Results show that cement materials from different production plants exhibit different mechanical and rheological behaviors. For example, cement powder produced in Texas and Louisiana exhibit different strength and rheology performances, though both of them are labeled type H cement. Cement powder is comprised of silicon dioxide, calcium oxide, aluminum oxide, iron oxide, magnesium oxide, etc. It still remains unclear which and how a specific component or several components in raw cement powder result in different cement performance. To find out this or these components would be highly recommended.

- Effect of Different CNTs on the Rheology and Mechanical Properties of Cement

CNTs can be classified into two different categories, single-walled carbon nanotubes (SWCNTs) and multi-walled carbon nanotubes (MWCNTs), based on their different layered structures. Each category of CNTs contains dozens of different CNTs types, according to their different diameters, number of layers, and length to diameter ratios. It would be valuable to compare the effect of different types of CNTs and find out a best one for improving cement strength properties.

- Optimization of CNTs Concentration

This project used the same concentration of CNTs (0.5%bwoc) for all cement systems. Results show that adding 0.5%bwoc CNTs enhances cement strength properties and reduces permeability of foam cement without significantly changes the rheological behavior of cement slurries. However, the optimum concentration of CNTs for improving cement mechanical properties is still unknown. It would be valuable to find a relationship of CNTs concentration vs.

strength enhancement, and find an optimized CNTs concentration for maximum strength reinforcement.

- Extend Tri-axial Tests to Higher Confining Pressures

This project only tested different cement systems under the confining pressures of 0, 500 and 1000psi. Finding the mechanical behaviors of cement and lightweight cement under higher confining pressures will be meaningful for providing recommendations for field cementing applications.

- Cement Failure Model

An observation in this project is that cement fractures do not have a frictional nature. Therefore, the theoretical models such as Mohr-Coulomb criterion, which requires measured friction angle for stress calculation, shall not be used as a failure criterion for estimation of cement strength under tri-axial loading conditions. Develop a comprehensive failure criterion which can simulate and predict cement failure is suggested.

- Cement Curing Conditions

In this study, all cement specimens were prepared under ambient conditions. Cure and test cement specimen under high pressure and high temperature conditions are recommended.

NOMENCLATURE

σ_a	Axial stress
ε_a	Axial strain
ε_r	Circumferential strain
E	Young's modulus
v	Poisson's Ratio
k	Absolute permeability
μ	Viscosity
Q	Stabilized flow rate across test specimen
A	Cross-sectional area of test specimen
L_t	Lateral length of tri-axial test specimen
ΔP	Pore pressure difference across test specimen
$\emptyset$	Porosity
V_{void}	Total volume of void spaces in test specimen
V_t	Volume of test specimen
T_o	Splitting tensile strength
F_{max}	Maximum load recorded during splitting tensile test
D	Diameter of test specimen
L_s	Lateral length of splitting tensile test specimen
x_i	Measured value for R^2 calculation
X_i	Model expected value for R^2 calculation

y_i	Measured value for $RMSE$ calculation
Y_i	Model expected value for $RMSE$ calculation
K	Consistency factor
n	Flow behavior index
τ_o	Yield stress
γ	Shear rate

BIBLIOGRAPHY

[1] Craft, B., Johnson, T., and Kirkpatrick, H.: "Effects of Temperature, Pressure and Water-cement Ratio on the Setting Time and Strength of Cement," Tulsa Meeting, (1935).

[2] McElfresh, P., and Boncan, V.: "Applications of Foam Cement," paper SPE 11203 presented at the 1982 57th Annual Fall Technical Conference and Exhibition of the Society of Petroleum Engineers of AIME, New Orleans, Louisiana, 26-29 September.

[3] Olanson, M.: "Application of Foam Cement in Alberta," Journal of Canadian Petroleum Technology, Montreal, Canada, (1985) 49-57.

[4] Ahmed, R., Takach, N., Khan, U., Taoutaou, S., James, S., Saasen, A., and Godoy, R.: "Rheology of Foamed cement," Cement and Concrete Research, 39 (2009) 353–361.

[5] Kopp, K., Reed, S., Foreman, J., Carty, B., and Griffith, J.: "Foamed Cement vs. Conventional Cement for Zonal Isolation – Case Histories," paper SPE 62895 presented at the 2000 SPE Annual Technical Conference and Exhibition, Dallas, Texas, 1-4 October.

[6] Bremner, T.: "Influences of Aggregate Structure on Low Density Concrete," Ph.D. dissertation, University of London, (1981).

[7] Lumsden, S., Singh, J., Morgan, R., and Hundt, G.: "Development and Rheological Characterization of Suspension of Hollow Glass Beads," paper SPE 181347 presented at the 2016 SPE Annual Technical Conference and Exhibition, Dubai, UAE, 26-28 September.

[8] Nelson, E., and Guillot, D.: "Well Cementing," Second Edition, (2006).

[9] Mata, C., and Calubayan, A.: "Use of Hollow Glass Spheres in Lightweight Cements - Selection Criteria," paper SPE 182399 presented at the 2016 SPE Asia Pacific Oil & Gas Conference and Exhibition, Perth, Australia, 25-27 October.

[10] D. Kulakofsky, R. Vargo, New Technology for the Delivery of Beaded Lightweight Cements, paper SPE 94541, presented at the 2005 SPE Annual Technical Conference and Exhibition, Dallas, Texas, 9-12 October.

[11] Yu, M., Lourie, O., Dyer, M., Moloni, K., Kelly, T., and Ruoff, R.: "Strength and Breaking Mechanism of Multiwalled Carbon Nanotubes under Tensile Load," Science, (2000) 287.

[12] Musso, S., Tulliani, J., Ferro, G., and Tagliaferro, A.: "Influence of carbon nanotube structure on the mechanical behavior of cement composites," Composites Science and Technology, 69 (2009) 1985–1990.

[13] Tyson, B., Abu Al-Rub, R., Yazdanbakhsh, A., and Grasley, Z.: "Carbon Nanotubes and Carbon Nanofibers for Enhancing the Mechanical Properties of Nanocomposite Cementitious Materials," Journal of Materials in Civil Engineering, (2011) 23.

[14] Rahimirad, M., and Baghbadorani, J.: "Properties of Oil Well Cement Reinforced by Carbon Nanotubes," paper SPE 156985 presented at the 2012 SPE International Oilfield Nanotechnology Conference, Noordwijk, Netherlands, 12-14 June.

[15] Khan, W., Rahman, M., Mahmoud, M., and Sarmah, P.: "MWCNT for Enhancing Mechanical Properties of Oil Well Cement for HPHT Applications," paper SPE/IADC 178175 presented at the 2016 SPE/IADC Middle East Drilling Technology Conference and Exhibition, Abu Dhabi, UAE, 26–28 January.

[16] Paula, J., Calixto, J., Ladeira, L., Ludvig, P., Souza, T., Rocha, J., and Melo, A.: "Mechanical and Rheological Behavior of Oil-well Cement Slurries Produced with Clinker

Containing Carbon Nanotubes," Journal of Petroleum Science and Engineering, 122(2014)274–279.

[17] Santra, A., Boul, P., and Pang, X.: "Influence of Nanomaterials in Oilwell Cement Hydration and Mechanical Properties," paper SPE 156937 presented at the 2012 SPE International Oilfield Nanotechnology Conference, Noordwijk, Netherlands, 12-14 June.

[18] Olowolagba, K., and Brenneis, C.: "Techniques for the Study of Foamed Cement," paper SPE 133050 presented at the 2010 SPE Production and Operations Conference and Exhibition, Tunis, Tunisia, 8-10 June.

[19] Griffith, J., Lende, G., Ravi, K., Saasen, A., Nodland, N., and Jordal, O.: "Foam Cement Engineering and Implementation for Cement Sheath Integrity at High Temperature and High Pressure," paper IADC/SPE 87194 presented at the 2004 IADC/SPE Drilling Conference, Dallas, Texas, 2-4 March.

[20] Dusterhoft, D.: "A Comparison Between Foamed and Lightweight Cements," paper PETSOC-2003-125 presented at the 2003 Canadian International Petroleum Conference, Calgary, Alberta, 10-12 June.

[21] Spaulding, R., Haljasmaa, I., Fazio, J., Gieger, C., Kutchko, B., Gardiner, J., Shine, J.M., Benge, G., DeBruijn, G., and Harbert, W.: "An Assessment of the Dynamic Moduli of Atmospherically Generated Foam Cements," paper OTC 25776 presented at the 2015 Offshore Technology Conference, Houston, Texas, 4-7 May.

[22] Kutchko, B., Crandall, D., Moore, J., Magdalena, G., Haljasmaa, I., Spaulding, R., Harbert, W., Benge, G., DeBruijn, G., and Shine, J.M.: "Assessment of Foamed Cement Used in Deep Offshore Wells," paper SPE 170298 presented at the 2014 SPE Deepwater Drilling and Completions Conference, Galveston, Texas, 10-11 September.

[23] Sarmah, P., Yadav, P., and Agrawal, G.: “High-Strength Lightweight Cement Optimized for Weak Formations - Use of Local Raw Material Improves Performance and Operational Latitude,” paper SPE 178038 presented at the 2015 SPE Oil & Gas India Conference and Exhibition, Mumbai, India, 24-26 November.

[24] Veisi, S., Taoutaou, S., Steven, A., Pasteris, M., Wedhaswari, R., Awalt, M., Kadrie, M., and Permata, E.: “Engineered Highly Crush-Resistant Cement Slurry to Prevent Lost Circulation,” paper SPE 176038 presented at the 2015 SPE/IATMI Asia Pacific Oil & Gas Conference and Exhibition, Nusa Dua, Bali, Indonesia, 20-22 October.

[25] Blake, B., Bowditch, R., Simacheva, N., Hudson, M., Crane, D., and Shea, C.: “Achieving Top of Cement; An Engineered Solution for Loss Zone Wells in the Bakken,” paper SPE 175918 presented at the 2015 SPE/CSUR Unconventional Resources Conference, Calgary, Alberta, Canada, 20-22 October.

[26] Tan, B., Lang, M., and Sheth, D.: “High-Strength, Low-Density Cement Pumped On-the-Fly using Volumetric Mixing Achieves Cement to Surface in Heavy Loss Coal Seam Gas Field,” paper SPE 158092 presented at the 2012 SPE Asia Pacific Oil and Gas Conference and Exhibition, Perth, Australia, 22-24 October.

[27] Kulakofsky, D., Avalos A., and Hernandez, R.: “Superior Zonal Isolation Provided by Ultra-Lightweight Cementing Technology Increases Profitability of Wells in Difficult to Cement Areas,” paper SPE 104066 presented at the 2006 SPE International Oil Conference and Exhibition, Cancun, Mexico, 31 August – 2 September.

[28] Koopman, M., Gouadec, G., Carlisle, K., Chawla K., and Gladysz, G.: "Compression Testing of Hollow Microspheres (Microballoons) to Obtain Mechanical Properties," Scripta Materialia, vol. 50, pp. 593-596, 2004.

[29] Carlisle, K., Chawla, K., Gladysz, G., and Koopman, M.: "Structure and Mechanical Properties of Micro and Macro Balloons: An Overview of Test Techniques," Journal of Materials Science, vol. 41, pp. 3961-3972, 2006.

[30] Hunter, T., Pugh, R., Franks, G., and Jameson, G.: "The Role of Particles in Stabilizing Foams and Emulsions," Advances in Colloid and Interface Science, vol. 137, pp. 57-81, 2008.

[31] Yang, Y., Grulke, E., Zhang, Z., and Wu, G.: "Thermal and Rheological Properties of Carbon Nanotube in Oil Dispersions," Journal of Applied Physics, vol. 99, 114307, 2006.

[32] Potschke, P., Fornes, T., and Paul, D.: "Rheological Behavior of Multiwalled Carbon Nanotube/Polycarbonate Composites," Polymer, vol.43, pp.3247-3255, 2002.

[33] Nazari, A., and Riahi, S.: "The Effect of SiO2 Nanoparticles on Physical and Mechanical Properties of High Strength Compacting Concrete," Composites, Part B. 2011.

[34] Li, G., Wang, P., and Zhao, X.: "Mechanical Behavior and Microstructure of Cement Composites Incorporating Surface-treated Multi-walled Carbon Nanotubes," Carbon, vol.43, pp. 1239-1245, 2005.

[35] Patil, R., and Deshpande, A.: "Use of Nanomaterials in Cementing Applications," paper SPE 155607 presented at the 2012 SPE International Oilfield Nanotechnology Conference and Exhibition, Noordwijk, The Netherlands, 12-14 June.

[36] Taiwo, O., and Ogbonna, J.: "Foam Cementing Design and Application: A Cure for Low Gradient-Associated Problems in Deepwater Operations in the Gulf of Guinea," paper SPE 150767 presented at 2011 Nigeria Annual International Conference and Exhibition, Abuja, Nigeria, 30 July - 3 August.

[37] Kawashima, S., Hou, P., Corr, D., and Shah, S.: "Modification of Cement-Based Materials with Nanoparticles," Cement & Concrete Composites, vol.36, pp. 8-15, 2013.

[38] API Specification 10A/ISO 10426-1, 2002, Specification for Cements and Materials for Well Cementing, 23th Edition.

[39] API Recommended Practice 10B-2, Recommended Practice for Testing Well Cements, 2nd Edition, 2010.

[40] API Recommended Practice 10B-4, Preparation and Testing of Foamed Cement Formulations at Atmospheric Pressure, 2nd Edition, 2015.

[41] ASTM D 4543, Standard Practices for Preparing Rock Core as Cylindrical Test Specimens and Verifying Conformance to Dimensional and Shape Tolerances, 2008.

[42] ASTM D 3967. Standard Test Method for Splitting Tensile Strength of Intact Rock Core Specimens, 2016.

[43] Reed, T., Pickell, B., and Volk, L.: Foam Generator and Viscometer Apparatus and Process, US Patent, US 6807849 B1, 2004.

[44] ASTM D 7012-04. Standard Test Method for Compressive Strength and Elastic Moduli of Intact Rock Core Specimens under Varying States of Stress and Temperatures, 2004.

[45] Hucka, V., and Das, B.: "Brittleness Determination of Rocks by Different Methods," International Journal of Rock Mechanics and Mining Sciences & Geomechanics Abstracts, vol. 11, issue 10, pp. 389-392, 1974.

[46] Zaitsev, Y., and Wittmann, F.: "Simulation of crack propagation and failure of concrete," Materials and Structures, 1981.

[47] Labuz, J., and Zang, A.: "Mohr-Coulomb Failure Criterion," Rock Mech Rock Eng, vol. 45, pp. 975-979, 2012.

[48] Alejano, L., and Bobet, A.: "Drucker-Prager Criterion," Rock Mech Rock Eng, vol. 45, pp. 995-999, 2012.

[49] Al-Ajmi, A., and Zimmerman, R.: "Stability Analysis of Vertical Boreholes Using the Mogi-Coulomb Failure Criterion," International Journal of Rock Mechanics and Mining Sciences, vol.43, pp. 1200-1211, 2006.

[50] Hoek, E., Carranza-Torres, C., and Corkum, B.: "Hoek-Brown Failure Criterion – 2002 Edition," Proc. NARMS-TAC Conference, Toronto, Canada, 2002.

[51] Chang, C., and Haimson, B.: "A Failure Criterion for Rocks Based on True Triaxial Testing," Rock Mech Rock Eng, vol. 45, pp. 1007-1010, 2012.

[52] Mindess, S., Young, J., and Darwin, D.: "Concrete," 2nd Edition, 2003.

[53] Girifalco, L., Hodak, M., and Lee, R.: "Carbon Nanotubes, Buckyballs, Ropes and a Universal Graphitic Potential," Physical Review B, vol.62, No.19, 2000.

APPENDIX A

MATLAB CODE FOR RHEOLOGY CHARACTERIZATIONS

```
clc;
clear all;
x=[ ];              %shear rate data
y1=[ ];             %shear stress data
scatter(x,y1,400,'*k')
hold on
 y2=[ ];            %shear stress data
scatter(x,y2,400,'xk')
hold on
 y3=[ ];            %shear stress data
scatter(x,y3,400,'sk')
hold on
y4=[ ];             %shear stress data
scatter(x,y4,400,'ok')
hold on

[x,I]=sort(x);y1=y1(I);y2=y2(I);y3=y3(I);y4=y4(I);
func1=@(a,x)a(1).*x.^(a(2))+a(3);          %Trend line Func.
func2=@(b,x)b(1).*x.^(b(2))+b(3);
func3=@(c,x)c(1).*x.^(c(2))+c(3);
func4=@(d,x)d(1).*x.^(d(2))+d(3);
a0=[0.001,0.001,0.001];                    %Assume initial value
m1=lsqcurvefit(func1,a0,x,y1);             %Add trend line.
b0=[0.001,0.001,0.001];
m2=lsqcurvefit(func2,b0,x,y2);
c0=[0.001,0.001,0.001];
m3=lsqcurvefit(func3,c0,x,y3);
d0=[0.001,0.001,0.001];
m4=lsqcurvefit(func4,c0,x,y4);

hold on
plot(x,m1(1)*x.^m1(2)+m1(3),'r-')          %Plot trend line
plot(x,m2(1)*x.^m2(2)+m2(3),'r--')
plot(x,m3(1)*x.^m3(2)+m3(3),'g-')
plot(x,m4(1)*x.^m4(2)+m4(3),'g--')
legend('  ')
xlabel('Shear Rate(1/s)')
```

```
ylabel('Shear Stress(Pa)')
set(gca,'FontSize',35);
disp(m1)                    %Display coefficients
disp(m2)
disp(m3)
disp(m4)
```